Journal of Microscopy, Vol. 226, Pt 2 May 2007, pp. 90–120
Received 23 August 2006; Accepted 12 December 2006

Fluorescence lifetime imaging microscopy of *Chlamydomonas reinhardtii*: non-photochemical quenching mutants and the effect of photosynthetic inhibitors on the slow chlorophyll fluorescence transient

O. HOLUB[*,†], M. J. SEUFFERHELD[§], C. GOHLKE[*,†], GOVINDJEE[**,¶], G. J. HEISS[*,‡] & R. M. CLEGG[*,¶]

[*] *Department of Physics, University of Illinois at Urbana-Champaign, 1110 West Green St., Urbana, IL 61801, U.S.A.*

[§] *Department of Natural Resources and Environmental Sciences (NRES), 311a Edward Madigan Lab, University of Illinois at Urbana-Champaign, 1201 West Gregory Drive, Urbana, IL 61801, U.S.A.*

[**] *Department of Plant Biology and of Biochemistry, 265 Morrill Hall, University of Illinois at Urbana-Champaign, 505 S Goodwin Ave., Urbana, IL 61801, U.S.A.*

¶ *Center of Biophysics and Computational Biology, University of Illinois at Urbana-Champaign, 607 S, Mathews Avenue, Urbana, IL 61801, U.S.A.*

† *Present Address: Laboratory for Fluorescence Dynamics, Biomedical Engineering Department, University of California, Irvine, 3206 Natural Sciences II Building, Irvine, CA 92697-2715, U.S.A.*

‡ *Institut für physikalische Chemie, AK Bräuchle Butenandstraße 1181377, München, Germany*

Key words. *Chlamydomonas*, FLI, FLIM, fluorescence induction, lifetime microscopy, lifetime of fluorescence, lifetime transient, non-photochemical quenching, npq1 mutant, npq2 mutant, polar plot, xanthophyll-cycle.

Summary

Fluorescence lifetime-resolved images of chlorophyll fluorescence were acquired at the maximum P-level and during the slower transient (up to 250 s, including P-S-M-T) in the green photosynthetic alga *Chlamydomonas reinhardtii*. At the P-level, wild type and the violaxanthin-accumulating mutant npq1 show similar fluorescence intensity and fluorescence lifetime-resolved images. The zeaxanthin-accumulating mutant npq2 displays reduced fluorescence intensity at the P-level (about 25–35% less) and corresponding lifetime-resolved frequency domain phase and modulation values compared to wild type/npq1. A two-component analysis of possible lifetime compositions shows that the reduction of the fluorescence intensity can be interpreted as an increase in the fraction of a short lifetime component. This supports the important photoprotection function of zeaxanthin in photosynthetic samples, and is consistent with the notion of a 'dimmer switch'. Similar, but quantitatively different, behaviour was observed in the intensity and fluorescence lifetime-resolved imaging measurements for cells that were treated with the electron transport inhibitor 3-(3,4-dichlorophenyl)-1,1-dimethyl urea, the efficient PSI electron acceptor methyl viologen and the protonophore nigericin and. Lower fluorescence intensities and lifetimes were observed for all npq2 mutant samples at the P-level and during the slow fluorescence transient, compared to wild type and the npq1 mutant.

The fluorescence lifetime-resolved measurements during the slow fluorescence changes after the P level up to 250 s for the wild type and the two mutants, in the presence and absence of the above inhibitors, were analyzed with a graphical procedure (polar plots) to determine lifetime compositions. At higher illumination intensity, wild type and npq1 cells show a rise in fluorescence intensity and corresponding rise in the species concentration of the slow lifetime component after the initial decrease following the P level. This reversal is absent in the npq2 mutant, and for all samples in the presence of the inhibitors. Lifetime heterogeneities were observed in experiments averaged over multiple cells as well as within single cells, and these were followed over time. Cells in the resting state (induced by several hours of darkness), instead of the normal swimming state, show shortened lifetimes. The above

Correspondence to: Robert Clegg. Tel: 1–217-244-8143; fax: 1–217244-7187; e-mail: rclegg@uiuc.edu

results are discussed in terms of a superposition of effects on electron transfer and protonation rates, on the so-called 'State Transitions', and on non-photochemical quenching. Our data indicate two major populations of chlorophyll a molecules, defined by two 'lifetime pools' centred on slower and faster fluorescence lifetimes.

1. Introduction

Photosynthetic organisms adapt to changes in environmental conditions in order to optimize their photosynthetic activity and minimize damage due to stress. Damaging reactive molecular species produced during excessive light intensity can be avoided by dissipating potentially harmful excess absorbed energy as heat. Non-photochemical quenching (NPQ) of chlorophyll (Chl) *a* fluorescence is a ubiquitous photoprotective mechanism in photosystem (PS) II, described in recent reviews (Gilmore & Govindjee, 1999; Horton *et al.*, 1999; Demmig-Adams & Adams III, 2000; Müller *et al.*, 2001; Govindjee & Seufferheld, 2002; Demmig-Adams *et al.*, 2006). These mechanisms take place over an extended time period, and involve several phases of photosynthesis.

Chlorophyll fluorescence lifetime measurements during the fluorescence transient were measured earlier in the green alga *Chlorella pyrenoidosa* (Briantais *et al.*, 1972) and plant leaves (Malkin *et al.*, 1980). Detailed studies with plant leaves and other photosynthetic systems were recently published (Malkin *et al.*, 1980; Moise & Moya, 2004a, b).

Imaging fluorescence intensity of photosynthetic systems has been extensively carried out (Nedbal & Witmarsh, 2004; Oxborough, 2004a, b). However, only fluorescence lifetime imaging can provide reliable information on the quantum yield of fluorescence related to rate constants of energy dissipation (Holub *et al.*, 2000). This paper deals with detailed fluorescence lifetime imaging measurements during the P-to-S-to-M to-T transient in untreated, and chemically treated *Chlamydomonas* cells and mutants. The fluorescence transient is a series of consecutive events defined as PSMT: P stands for the initial peak of fluorescence after initial illumination, S for a semi-steady state (which has fluorescence intensity lower than the P state), M for a possible maximum in fluorescence following the S state, and T for a terminal steady state with lower fluorescence intensity than the M state (Papageorgiou, 1975).

1.1. General scheme of photosynthesis and pathways of de-excitation from the excited state of chlorophyll

Figure 1 is a diagrammatic overview of the major components of the photosynthetic reaction scheme (Wydrzynski & Satoh, 2005; Golbeck, 2006). The steps of the photosynthetic scheme that are acted on by the inhibitors of photosynthesis, 3(3,4-dichloro-phenyl)-1,1-dimethyl urea (DCMU), nigericin, and methyl viologen are also indicated. Light is absorbed by Chls, and carotenoids, which are located in several pigment-protein complexes, especially in the light-harvesting complexes (LHCs) of the two photosystems PSI and PSII in the thylakoid membranes of the chloroplasts (Green & Parson, 2003).

Several competitive pathways are available for electronically excited Chl molecules to return to their ground state (Lakowicz, 1999; Papageorgiou & Govindjee, 2004): (1) fluorescence; (2) rapid energy migration between Chl molecules from the antenna system to the reaction centre and hetero-transfer between Chl and other molecules, both by Förster resonance energy transfer (FRET); (3) primary photochemistry; (4) binding interactions; (5) heat dissipation *via* internal conversion; (6) intersystem crossing from the Chl singlet-state to the Chl triplet-state and (7) transfer of energy from the excited triplet state of Chl to the ground-state of oxygen (a triplet). The last pathway generates singlet-state oxygen, which can damage important biological processes and subsequently can produce other damaging reactive species (radicals).

Because the de-excitation pathways are kinetically competitive, Chl fluorescence can be used to monitor many of the non-fluorescent photochemical reactions of photosynthesis. Deactivation pathways involving direct quenching of the excited state by a photochemical pathway are defined as photochemical quenching, qP. All other deactivation pathways are collectively defined as NPQ. If the intrinsic rate of fluorescence is constant, changes in the fluorescence emission caused by NPQ directly reveal quantitative properties of photosynthesis (Govindjee, 2004).

1.2. Non-photochemical quenching

NPQ is classified into three types according to their relaxation times and mechanisms (Müller *et al.*, 2001): (a) Energy-dependent quenching (qE) takes place through charge separation at the reaction centre; qE happens in seconds to minutes and requires the build-up of a transthylakoid proton gradient (Demmig-Adams, 2003; Yamamoto, 2006). (b) Quenching involving a transition from state 1 to state 2 (qT) is brought about by movement of specific LHCs from the more fluorescent PSII to the lower fluorescent PSI region; this process relaxes in tens of minutes (Allen & Forsberg, 2001; Allen, 2002); qT decreases the antenna size of PSII and increases the antenna size of PSI (Takahashi *et al.*, 2006), thereby shifting the photosynthetic system from a high fluorescent 'state 1' to a low fluorescent 'state 2'. Changes in state can take place in the reverse direction as well. (c) Photoinhibitory quenching (qI) is often very slow, sometimes lasting hours (Adir *et al.*, 2003; Matsubara & Chow, 2004; Osmond & Forster, 2006). In this report we are concerned mainly with qE and qT. A frequency domain lifetime study of qI studying changes over several hours has been reported recently with leaf segments of *Capsicum annuum L* (Matsubara & Chow, 2004).

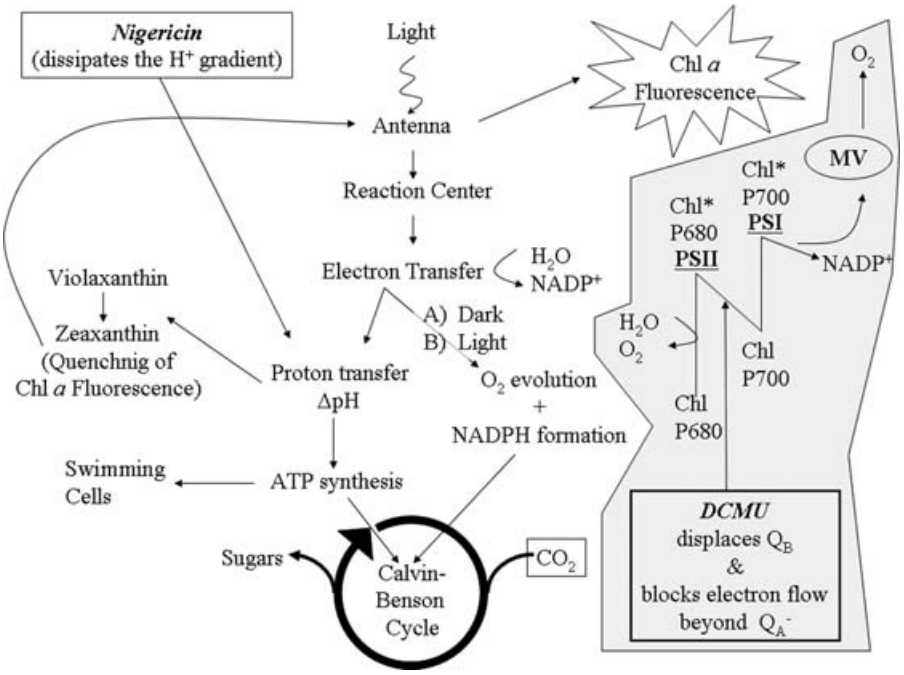

Fig. 1. A diagram indicating the interference in the photosynthesis mechanism by DCMU, nigericin and methyl viologen. The diagram presents schematic of the photosynthetic reactions, and the possible sites of DCMU, nigericin and methyl viologen inhibition. The electron transfer inhibitor DCMU is known to replace the plastoquinone Q_B of PSII, closing the PSII reaction centre and blocking electron transport from PSII to PSI. The protonophore nigericin dissipates the proton gradient of the thylakoid membrane (among other effects). Methyl viologen is one of the most efficient electron acceptors of PSI. Its removal of electrons prevents the usual 'blockage' of the electron flow during photosynthesis and thereby the accumulation of reduced Q_A.

1.3. Energy-dependent quenching

qE is usually associated with the activation of the xanthophyll cycle (Demmig *et al.*, 1988; Demmig-Adams *et al.*, 1996; Demmig-Adams *et al.*, 2006). Under intense irradiation, exceeding a plant's capacity for CO_2 fixation, lumen acidification leads to the enzymatic conversion of violaxanthin to zeaxanthin *via* the intermediate antheraxanthin. The build-up of the ΔpH across the thylakoid membrane leads to protonation reactions and possible conformational changes in one or more of the antenna pigment-proteins of PSII, which favour the binding of zeaxanthin. The combination of these two events is thought to lead to a quenched state of PSII fluorescence with shorter fluorescence lifetimes and lowered Chl fluorescence intensity (Gilmore *et al.*, 1995; Gilmore *et al.*, 1998). Conformational changes in the thylakoid membrane have been inferred from the lifetime measurements (Gilmore *et al.*, 1998) and from absorbance changes at 535 nm (ΔA_{535nm}) (Krause, 1973; Bilger & Björkman, 1994; Mohanty *et al.*, 1995). These conformational changes are correlated with changes in the PSII protein *PsbS* (Li *et al.*, 2000). The minor Chl-protein complexes (CP26, CP29) (Bassi *et al.*, 1993; Andersson *et al.*, 2001; Crimi *et al.*, 2001; Frank *et al.*, 2001), and a light harvesting polypeptide *Lhcbm1* are also involved (Elrad *et al.*, 2002).

Numerous environmental effects and molecular interactions affecting qE have been investigated. Isolated thylakoid membranes exhibit qE in the absence of zeaxanthin, but only at lumen pH values lower than normal *in vivo* conditions (Rees *et al.*, 1992; Kramer *et al.*, 2004; Cruz *et al.*, 2005). Quenching can also be induced by zeaxanthin even without ΔpH in isolated LHCs of PSII (Wentworth *et al.*, 2000). Inhibition of qE could be observed when the zeaxanthin synthesis was blocked *in vivo* (Horton *et al.*, 1994). Antheraxanthin also plays a role in qE (Gilmore & Yamamoto, 1993; Gilmore *et al.*, 1998) and can partially replace the role of zeaxanthin in certain algae (Goss & Boehme, 1998). In some cases, another xanthophyll, lutein, seems also to be involved (Niyogi *et al.*, 1997, 2001).

In general, the level of quenching of Chl fluorescence correlates with the amount of zeaxanthin (Demmig-Adams, 1990). Many details of the mechanism of Chl de-excitation by xanthophylls are not known. The role of the xanthophylls could be indirect, affecting a structural antenna rearrangement by inducing conformational changes in the antenna complexes, which subsequently quench excited Chl. This could disrupt energy transfer pathways. Exciplex formation or a combination of dynamic quenching (collisional shortening of the lifetime) and static quenching (no change in the fluorescence lifetime) could participate.

Excited Chl molecules could be quenched by a change in the environment surrounding the Chls by increasing the rate of internal conversion. Or if there is close association of Chl and xanthophylls, energy could be transferred non-radiatively from Chl to zeaxanthin (Förster energy transfer). Hetero FRET is in principle possible between Chl and zeathanthin, because the lowest singlet excited state S_1 of Chl *a* is higher than the S_1 states of the xanthophylls (Polívka *et al.*, 1999; Frank *et al.*, 2000; Polívka *et al.*, 2002). However, the question still remains whether transfer to zeaxanthin is more efficient than violaxanthin; a recent publication indicates that violaxanthin quenches much weaker than zeaxanthin (Avital *et al.*, 2006). This depends not only on the energy levels, but also on the distance between the donor and the acceptor molecules and the orientations of molecules with respect to each other. Furthermore, the nature of the role of zeaxanthin in the de-excitation of Chl may involve formation of a cation of this carotenoid (Holt *et al.*, 2005).

1.4. NPQ mutants and previous studies

The isolation of mutants presented new possibilities for *in vivo* studies of NPQ (Niyogi, 1999). Two of these mutants are investigated in this work. The mutant npq1 is deficient in violaxanthin de-epoxidase; therefore, it is unable to convert violaxanthin to antheraxanthin and zeaxanthin (Niyogi *et al.*, 1997). The npq1 mutant accumulates violaxanthin and lacks zeaxanthin/antheraxanthin. The mutant npq2 is deficient in zeaxanthin epoxidase; therefore, it is unable to convert zeaxanthin to antheraxanthin and violaxanthin. This mutant accumulates zeaxanthin and lacks violaxanthin /antheraxanthin.

The npq1 and npq2 mutants and the wild type (WT; without cell walls) have been characterized (Niyogi *et al.*, 1997). At high excitation light intensities, lower rates of oxygen evolution were observed for the violaxanthin-accumulating npq1 in comparison to WT (Govindjee & Seufferheld, 2002). The zeaxanthin-accumulating npq2 mutant showed rates of oxygen evolution similar to the WT. This might be an indication for antioxidant action of zeaxanthin in addition to its direct quenching properties. The lack of zeaxanthin in npq1 would then result in less photoprotection. The zeaxanthin-accumulating npq2 mutant shows a strong steady-state fluorescence quenching (Govindjee & Seufferheld, 2002), as measured with a pulse-amplitude-modulation instrument (Schreiber, 2004). This was found not only for untreated cells, but even those treated with an inhibitor of the electron transport, DCMU (3-(3,4-dichlorophenyl)-1,1-dimethyl urea). On the other hand, the npq1 mutant still showed a steady-state level of fluorescence similar to that in WT cells. Furthermore, several measurements by K.K. Niyogi and his collaborators have established that a PsbS protein plays a crucial role in the process of NPQ (Li *et al.*, 2004). However, molecular details of the entire process still remain to be discovered.

The quenching of Chl fluorescence can also be observed directly by measuring the initial (after dark adaptation) and maximum levels of the short time fluorescence transient of dark adapted cells (Govindjee, 2002). When photosynthetic organisms are irradiated after dark adaptation, the fluorescence intensity undergoes distinctive changes with time. This 'fluorescence induction', or 'fluorescence transient', is known as the Kautsky effect (Kautsky & Hirsch, 1931; Govindjee, 1995; Lazar, 1999). It is mainly a manifestation of the kinetics of electron transfer in PS II. It is affected by protonation events and by PSI activities. Significantly reduced fluorescence intensity (about 25–35% at P-level) has been detected for the npq2 mutant in comparison to the WT and the npq1 mutant (both of which showed about similar levels) even in the presence of the electron transport inhibitor DCMU and the proton gradient uncoupler, nigericin (Govindjee & Seufferheld, 2002).

Unfortunately, these results cannot be interpreted unambiguously. For instance, the npq2 cells had a 20% higher level of the measured initial fluorescence, F_{0meas}, in comparison to the WT and the npq1 cells, in spite of a higher level of NPQ in npq2. The operational definition of the extent of NPQ depends on the normalization with F_0 when one is measuring only fluorescence intensities. Due to the higher zeaxanthin concentration in npq2, one might have expected a quenching of F_{0meas}. The reason for this difference is not known (Govindjee & Seufferheld, 2002). The F_0 fluorescence intensity has multiple origins (85–90% from PSII centred at 685 nm and 10–15% from PS1 centred at 712 nm at room temperature). If some antennae complexes were to dissociate from the reaction centre core, this would lead to a decrease in the transfer of energy to the reaction centre core and to an apparently increased F_0. Lifetime measurements allow a comparison between the mutants, which is independent of any F_0 normalization.

When steady-state fluorescence intensities are measured, changes in the absorption cross-section of the PSII antenna (changes in concentration) cannot be distinguished from true differences in the quantum yield of fluorescence. State transitions (movement of specific pigment-protein antenna from PSII to PSI, and its reversal) (Delosme *et al.*, 1996; Bruce & Vasilev, 2004) might change the fluorescence intensities and give rise to erroneous interpretations if such processes are not taken into account. In this work we attempt to clarify these ambiguities by measuring lifetime-resolved fluorescence. Information about the quantum yield using fluorescence lifetime-resolved measurements should resolve some of these uncertainties and lead to a better understanding of many aspects of photosynthesis (Malkin *et al.*, 1980; Moya *et al.*, 2001), including the NPQ mechanism. Preliminary measurements on

fluorescence lifetime-resolved imaging (FLI) of *Chlamydomonas reinhardtii* cells (Holub *et al.*, 2000) have shown the importance of measuring lifetime-resolved fluorescence signals.

1.5. Rapid fluorescence lifetime-resolved imaging measurements

Fluorescence intensity transients in the millisecond to many-second time range are characteristic of photosynthetic samples following initial irradiation. Thus, it was necessary to carry out the FLI measurements rapidly in order to capture the lifetime changes in real time. Significant intensity changes must be negligible in the interval required for a complete measurement of each FLI time point. The FLI instrument has been described (Holub *et al.*, 2000; Clegg *et al.*, 2003) and has been optimized to minimize the time of acquisition and display. We have made FLI measurements at the P-level of the initial transient, and during the subsequent relaxation to the steady-state level. These latter changes are referred to as the P-to-S(T) decay, where, as noted earlier, P stands for peak and S for steady state (Lavorel, 1959; Krause, 1973; Briantais *et al.*, 1980). However, under some experimental conditions, a second wave of fluorescence is observed; that is, there is a rise from the S level to another maximum (M) level (Papageorgiou & Govindjee, 1968b; Mohanty & Govindjee, 1973) followed by a decay to a T level, the terminal state level. The S level then is a quasi steady-state level (Govindjee & Papageorgiou, 1971; Papageorgiou, 1975; Govindjee *et al.*, 1986).

FLI experiments were carried out on the two xanthophyll cycle mutants (npq1 and npq2) and WT cells. These imaging measurements were carried out with untreated cells and with cells treated with DCMU (an inhibitor of electron flow), methyl viologen (an efficient electron acceptor) and nigericin (an inhibitor of the proton gradient) (Fig. 1). Similar FLI measurements were also made with ensembles of cells in micro-capillaries to observe the algae under swimming and resting conditions. Extensive FLI measurements with WT and mutant cells, untreated and treated with the above chemicals, were carried out during the slow (from milliseconds to 250 s) fluorescence transient (P-to-S-to-M transient) during constant illumination.

2. Materials and Methods

2.1. Instrumentation

Fluorescence lifetime-resolved imaging experiments in the frequency domain, and the analysis of the lifetime-resolved data, are explained in detail in the Sections 2.1 and 2.2. Detailed descriptions of the instrument have been published (Holub *et al.*, 2000; Clegg *et al.*, 2003; Redford & Clegg, 2005a).

2.1.1. Analyzing multiple lifetimes with a single frequency. If some of the fluorescence lifetimes are constant throughout the measurement of the phase and modulation, it is possible to analyze single frequency lifetime-resolved measurements in terms of multiple lifetime components. The speed of the data acquisition during the P-to-S transient precludes acquiring multi-frequency data, in order to avoid large changes in the signals over the time of measurement, which would cause artefacts. We have carried out two such analyses of the phase and modulation measurements assuming two lifetime distributions. Both methods assume that a fast component exists with a short fluorescence lifetime, chosen to be between 0.3 and 0.4 ns, and which remains constant throughout the kinetic measurement. The first method, assuming only two lifetimes, calculates analytically the fraction of each component as well as the second (slower) lifetime. The second method [polar plot analysis (Redford & Clegg, 2005b); see Section 3.6] is similar, but is visually insightful, and can be carried out without a complex analytical calculation. The two lifetime analyses yield identical parameters, as they are analytically equivalent. Assumed lifetimes are based on previous measured lifetimes from a variety of photosynthetic systems (see Section 3.9). Multi-component analyses were carried out in order to gain a better understanding of possible contributions of separate lifetime components during the P-to-S transition, and the effect of the npq1 and npq2 mutations, as well as the inhibitors, on the underlying molecular mechanisms. We have also used the polar plot analysis to calculate the fractional contributions of three lifetimes, under the assumption that all three lifetimes are known and remain constant.

2.1.2. Recording the phase and modulation in the frequency domain. If a fluorescent sample is excited by sinusoidally modulated light, $E(t) = E_0 + E_{\omega_{HF}} \sin(\omega_{HF} t + \varphi_E)$, the detected fluorescence signal is modulated at the same frequency (Gratton & Limkeman, 1983; Lakowicz *et al.*, 1987; Clegg & Schneider, 1996) but with a different phase and modulation depth:

$$\begin{aligned} F_{\sin}(t) &= F_0 + F_{\omega_{HF}} \sin(\omega_{HF} t + \varphi_F - \varphi_E) \\ &= F_0 + F_{\omega_{HF}} \sin(\omega_{HF} t + \varphi). \end{aligned} \quad (1)$$

The expression ω_{HF} is the high frequency radial modulation frequency of the excitation light, and is usually between 1×10^7 and 1×10^8 cycles/s. The depth of modulation of the fluorescence signal is $M = [F_{\omega_{HF}}/F_0]/[E_{\omega_{HF}}/E_0]$ and $\varphi = \varphi_F - \varphi_E$ is the phase shift of the fluorescence measurement φ_f relative to the phase of the excitation light, φ_E.

For a simple sine wave excitation of the form

$$E(t) = E_0 + 2E_1 \cos(\omega t) = E_0 + E_1(e^{i\omega t} + e^{-i\omega t}), \quad (2)$$

the fluorescence response of a fluorophore with a single lifetime

reduces to

$$\begin{aligned} F(t) &= F_0 + F_1(\omega)\cos(\omega t + \phi) \\ &= Q\int_0^t (E_0 + 2E_1\cos(\omega t))\,Ae^{-(t-t')/\tau}dt' \\ &= Q\left[E_0 A\tau + E_1\left(\frac{2A\tau}{\sqrt{1+(\omega t)^2}}\cos(\omega\tau + \tan^{-1}(\omega\tau))\right)\right] \\ &= Q\,A\tau[E_0 + 2ME_1\cos(\omega\tau + \phi)]. \end{aligned} \quad (3)$$

In Eq. 3 for a single relaxing fluorescence component,

$$M = \frac{F_1(\omega)/F_0}{E_1/E_0} = \frac{1}{\sqrt{1+(\omega\tau)^2}}. \quad (4)$$

and

$$\phi = \tan^{-1}(\omega\tau). \quad (5)$$

The expressions M and ϕ are the demodulation and phase shift of the luminescence signal relative to the excitation light. As the frequency increases, the modulation depth decreases toward zero and the phase increases to a maximum of $\pi/2$. By measuring the modulation depth and the phase at many frequencies, the lifetime can be determined. Two independent lifetime parameters are determined, τ_M from Eq. 4, and τ_ϕ from Eq. 5.

Our frequency-domain fluorescence lifetime imaging system collects the full-field lifetime-resolved image; that is, the lifetime measurements are carried out at all pixels of the charged coupled device (CCD) simultaneously. Sustained rates of up to 26 fluorescence lifetime images per second can be obtained for images of 320 × 220 pixels. The dynamic waveforms of the excitation light and the fluorescence signal were repetitively sinusoidal. We employed the homodyne technique of measurement, where the amplification of the detector is modulated at the exact frequency of the excitation light. In the FLI case, the detector being modulated is an image intensifier, which is placed right before the CCD camera. The high frequency modulation of the light intensity and the amplification of the image intensifier were phase locked for homodyne operation (Clegg & Schneider, 1996; Clegg *et al.*, 1996, 2003) The phase and modulation of the fluorescence signal were determined by varying the phase of the intensifier amplification through one period of the high frequency modulation, and recording the static signal at every phase setting. The phase and modulation of the resulting homodyne sinusoidal recording is identical to that of the original high-frequency fluorescence signal. The phase and modulation at the fundamental repetitive frequency of the fluorescence signal at each pixel was determined rapidly and non-iteratively using a discrete Fourier Transform (Redford & Clegg, 2005a); this is equivalent to a least-squares regression using a sinusoid function to fit the data (Hamming, 1973).

The software (FlimFast) controlling the FLI data acquisition, analysis and display is interactive and enables video-rate image acquisition, data analysis and visualization of fluorescence lifetime images. Software functions can be altered during run-time with a minimum latency feedback and immediate data visualization; for example, multi-textured shaded surface renderings assist by providing a highly integrated view of the multi-parameter image data.

The modulation of the laser light at high frequency was performed with an acousto-optical modulator. The phase of the modulation of the image intensifier was digitally controlled by delay-line phase shifters. The data are rapidly transferred from the CCD to the computer and analyzed to determine the phase and modulation values at each pixel by digital Fourier analysis. The error of the Fourier analysis is determined from the variance of the difference between the recorded sinusoidal signal and the digital fit. This is possible because the excitation is well represented by a sinusoid.

The speed of the data acquisition depends on the number of consecutive phase-shifted images (at least three are required) and the time of integration at each phase setting (see Section 2.3). All phase-delayed images are recorded and saved, so that multi-pixel analysis of selected image regions can be performed later if desired. Pixels can be binned and averaged before the digital Fourier analysis of the consecutive images; this was carried out for the images containing large numbers of cells, which were not spatially resolved. As discussed in Section 3.10 (single cell resolution), the cells showed predominately homogeneous phase and modulation values. A single lifetime-resolved image (fitting all pixels separately) can be acquired in 125 ms (this rate is limited by the camera).

2.2. *Phase and modulation,* τ_{phase} and τ_{mod}, *and multi-component analysis*

The degree of phase delay and the extent of demodulation of the fluorescence signal at the high frequency depend on the frequency of modulation and the fluorescence lifetimes (Bailey & Rollefson, 1953; Merkelo *et al.*, 1969; Jameson & Gratton, 1983; Clegg & Schneider, 1996; Clegg *et al.*, 1996). The phase and modulation are calculated at each pixel of the CCD from the set of images taken at several phase settings, and the lifetime-resolved images are then displayed. The calculated lifetimes τ_{phase} and τ_{mod} obtained from Eqs 4 and 5 are simply mathematical transformations, and portray the phase and modulation values on a time scale (Clegg & Schneider, 1996). Only in the case of a single lifetime component do the values of τ_{phase} and τ_{mod} correspond to true lifetimes; nevertheless, they are convenient representations of the measured phase and modulation parameters. We will use the phase and modulation parameters, and τ_{phase} and τ_{mod}, interchangeably throughout the text to present lifetime-resolved images. When more than one lifetime component is present, τ_{phase} is less than τ_{mod}.

We refer the reader to Sections 3.6.1 and 3.6.2 for a description of our multi-lifetime component data analysis. The analysis is represented as a 'polar plot'. This representation

is particularly helpful when studying complex biological systems, which change dynamically during the data acquisition (in this case, during the P-to-S-to-M transition). With the assumption that one lifetime is known, the intensity at every time point can be simulated within a multiplicative constant from the fractional amplitudes and lifetimes. The simulated intensities for all points of any individual kinetic curve all have the same multiplicative constant, such that the averages over the transient are the same for the simulated and measured intensities. Details of the calculation of the simulated intensities are in Section 3.6.4.

2.3. Experimental conditions for the fluorescence lifetime measurements

The 488 nm line of the argon-ion laser was modulated at a frequency of 80.652 MHz. A Zeiss Axiovert 135 inverted microscope (Carl Zeiss, Jena, Germany) was used for the measurements (Holub *et al.*, 2000). The wavelength range of the fluorescence emission was 690 ± 40 nm (band pass filter for fluorescence emission, Omega XF70/690DF40; Omega Optical, Brattleboro, Vermont). The intensity of the excitation light was adjusted by neutral density filters and ranged between 50 and 8600 μmol photons m^{-2} s^{-1}. For most experiments reported, the intensity was between 300 and 2500–2750 μmol photons m^{-2} s^{-1}. We refer in the text to the 'lower' (300 μmol photons m^{-2} s^{-1}) and 'higher' (2500 μmol photons m^{-2} s^{-1}) excitation light intensities. These latter two intensities are identified in the text and figures as 'Lo' and 'Hi', respectively. The cells were treated identically for all measurements, and were dark adapted for at least 5 min before each measurement.

2.3.1. P-level measurements. After dark adaptation, the cells were pre-exposed to the light for 1 s before 8, 16 or 32 incrementally phase-delayed images were acquired. Each image was averaged for 100 ms, so that the total illumination time of the measurement was about 1, 2.1 or 3.9 s. The timing of the measurement was chosen to remain within the constant plateau region of the transient maximum (the 'P' level). The lifetime-resolved measurements were carried out rapidly to avoid transient intensity changes during the time of measurement (Holub *et al.*, 2000; Redford & Clegg, 2005a). For all ensemble measurements (samples on nitrocellulose filter paper, micro-capillaries and lifetime transients), an objective magnification of ×10 was used. The single cell measurements were made with a 100× objective.

2.3.2. P-to-S-to-M fluorescence transient measurements. Lifetime-resolved measurements of the P-to-S-to-M fluorescence transient, recorded up to 250 s, were begun at the P-level fluorescence. Eight incrementally phase delayed measurements were taken at 100 ms intervals, and the measurement time for each transient time point was 0.9 s. This measurement time for each single time point was sufficiently rapid to study the P-to-S fluorescence decline. Selected multiple pixels of the homodyne FLI measurement were averaged at each phase setting and analyzed simultaneously. The fluorescence from multiple cells immobilized on nitrocellulose filter paper was also measured simultaneously at low magnification (×10 objective), where the signal at every pixel is an average from many cells.

2.4. Instrument calibration with a lifetime standard

The lifetime measurements were calibrated either against the phase and modulation depth of the excitation light, or from a fluorescent sample with known lifetime. A convenient, robust and accurate standard is a fluorescent plastic standard (in our case we used a purple CD SlimLine jewel case; InterAct, Florida), which was selected for its spectral emission at 690 ± 40 nm. This standard sample has reproducible phase and modulation values of $\tau_{phase} = 1.02$ ns and $\tau_{mod} = 1.26$ ns. These values were determined relative to two well-known standards in micro-capillaries: fluorescein in NaOH, which has a single-exponential lifetime of 4.1 ns (Sjöback *et al.*, 1995), and rhodamine 101 (Lambda Physik GmbH, Göttingen, Germany) that has a temperature-independent single-exponential lifetime of 4.34 ns in ethanol (Drexhage, 1973; Karstens & Kobs, 1980; Vogel *et al.*, 1988).

The instrument was calibrated before each measurement. For the data shown in Fig. 3, a single component digital Fourier analysis of the data was carried out on the average intensity from multiple selected pixels at every phase setting. The software module repeatedly acquires, analyzes and displays mean image statistics over time, to check on the phase-stability. After each sample measurement, the procedure was repeated on the standard to assure phase stability during the measurement, which is of special importance for the acquired time series of lifetime measurements.

2.5. Determination of the excitation light intensity

The radiant flux was measured with a radiant power meter (model 70260 with 70286 Si diode detector; Oriel Instruments, Stratford, Connecticut) directly in the focal plane of the objective. The illumination intensity profile was Gaussian, due to the use of a single mode fibre. With a thin and homogeneous layer of a fluorescent sample and a micro scale, the Gaussian profile was measured under the microscope. The area under the normalized Gauss curve, determined from a fit of the illumination profile, corresponds to the diameter of a (hypothetical) circular area of constant irradiation. This area was determined once for the objective, and thus the photon flux density in the centre of the image was directly calculated from the total radiant power measurement. The centre of the image illumination was used for studying the P-to-S-to-M Chl fluorescence transient in our *Chlamydomonas* samples.

We measured diameters of 79/650 μm for 100×/10× objectives. The irradiation variations in the image were dependent on the zoom optics used in the microscope. Therefore, lifetime measurements over a limited range of excitation intensities were possible in a single image.

2.6. *Algal growth conditions and measurement preparation*

Cells of the green alga *Chlamydomonas reinhardtii* were grown at 25° C photoheterotrophically, during constant illumination with 100 μmol photons m^{-2} s^{-1}, in tris-acetate phosphate TAP medium (12.0 mM Tris; 17.4 mM acetate; 7.0 mM NH_4Cl, 0.4 mM $MgSO_4$, 0.3 mM $CaCl_2$, 1 mM phosphate buffer, 1 ml/L Hunter's trace metal elements; the medium was adjusted to pH 7, with 1ml/L glacial acetic acid) (Harris, 1989). Cells in the tris-acetate phosphate medium were grown in Erlenmeyer flasks, and kept under motion (either on a circularly rotating shaker table or with a magnetic stirrer) until the measurement was performed. They were harvested in their late logarithmic growth phase. Under these conditions the cells showed high motility and high-photosynthetic activity. When high salt (HS) medium was used, it was 9.0 mM NH_4Cl, 0.08 mM MgCl, 9.0 mM NH_4Cl, 0.06 mM $CaCl_2$, 13.5 mM phosphate buffer (Sueoka, 1960).

The experiments, as well as the additions of the three photosynthetic inhibitors, were performed at room temperature. Nigericin (Sigma; St. Louis, Missouri), which dissipates the proton gradient across membranes (Gilmore & Yamamoto, 2001; Finazzi *et al.*, 2003) was added to the cell suspension (10 μM final concentration; 10 min incubation) after cells had been centrifuged down and the buffer was changed to the minimum HS medium (Sueoka, 1960; Harris, 1989). Methyl viologen (Gramoxone, Sigma), which accepts electrons from Photosystem I (Hiyama & Ke, 1971), was added to the cell suspension (100 μM final concentration), followed by a 10 min incubation. DCMU (diuron; Sigma), which inhibits photosynthetic electron transfer between Q_A and the cytochrome b_6f complex by replacing plastoquinone Q_B of PSII (Velthuys, 1981; Wraight, 1981), was added in darkness (after 5 min dark adaptation) to the cell suspension (10 μM final concentration), followed by a 5 min incubation in the dark prior to the fluorescence lifetime measurements.

The slow fluorescence transient has been measured previously from an ensemble of algal cells suspended in buffer (Govindjee & Seufferheld, 2002). We have used three different experimental procedures to measure the fluorescence signals from an ensemble of cells at low magnification. Similar procedures were also used for single cell observations in combination with high-magnification optics and reduced cell numbers. The three procedures were:

(1) A sufficiently large number of cells were deposited from a suspension of cells on a nitrocellulose filter paper, pore size 1.2 μm (Millipore; Bedford, Massachusetts), which had been previously soaked in minimum HS medium, using a mild vacuum, such that they form a continuous layer of immobilized cells. This avoids movement of the cells out of the focus under the microscope due to the water uptake by the filter. The filter was then covered with minimum HS medium (pH 7) and a cover slip. For comparative measurements, the filter paper with deposited WT, npq1 and npq2 was cut and arranged under a single cover slip.

(2) The cells were filled into rectangular micro-capillaries. Before placing the cells into micro-capillaries (precision rectangle glass capillary tubes, microslides or Vitrotubes; inner diameter 0.03 × 0.3 mm; VitroCom, Inc., Mountain Lakes, New Jersey), the cell suspension was centrifuged, the supernatant nearly completely removed, and then the cells were re-suspended in the drop of medium left in the tube. This produced a highly concentrated cell suspension in the capillaries.

(3) The cells were deposited onto a thin film of agar between two microscope cover slips. Thin agar films were formed by applying a drop of warm agar (agar bacteriological; Sigma), prepared with HS medium, between two large microscope cover slips. After cooling, one cover slip could be lifted, the cell suspension was applied and then it was covered by the cover slip.

The first and the second method offer direct comparison of the xanthophyll cycle mutants and WT in a single image, allowing an accurate differential measurement. Pieces of filter paper with the different cells were cut out, and arranged side by side under the microscope, or by putting the three micro-slides next to each other in the same field of view (Fig. 2). Procedures 2 and 3 also allowed transmission light images to be recorded, whereas with the first method only the Chl fluorescence could be observed. In procedure 2, the cells are not immobilized. Single cell lifetime measurements were carried out on cells that have stopped their movement (as discussed later). Ensemble measurements of swimming cells were made, because the cell number was high and the spatial resolution sufficiently low such that the average signal was not affected any more by movement of single cells during the measurement time.

At the beginning of a series of microscope measurements, the cells were briefly illuminated with 'Lo' light intensity (300 μmol photons m^{-2} s^{-1}) for focusing purposes. Then the cells were illuminated briefly with the chosen excitation light intensity [300 ('Lo') or 2500 ('Hi') μmol photons m^{-2} s^{-1}] to adjust the image intensifier gain for an optimal dynamic range of the camera. This was followed by dark adaptation of the cells for 5 min. For the acquisition of a series of measurements the gain adjustment had to be performed only once.

2.7. *Characteristic effects of DCMU, nigericin and methyl viologen*

DCMU: DCMU is a herbicide. As noted earlier, it replaces the plastoquinone Q_B of PSII, thereby blocking the electron

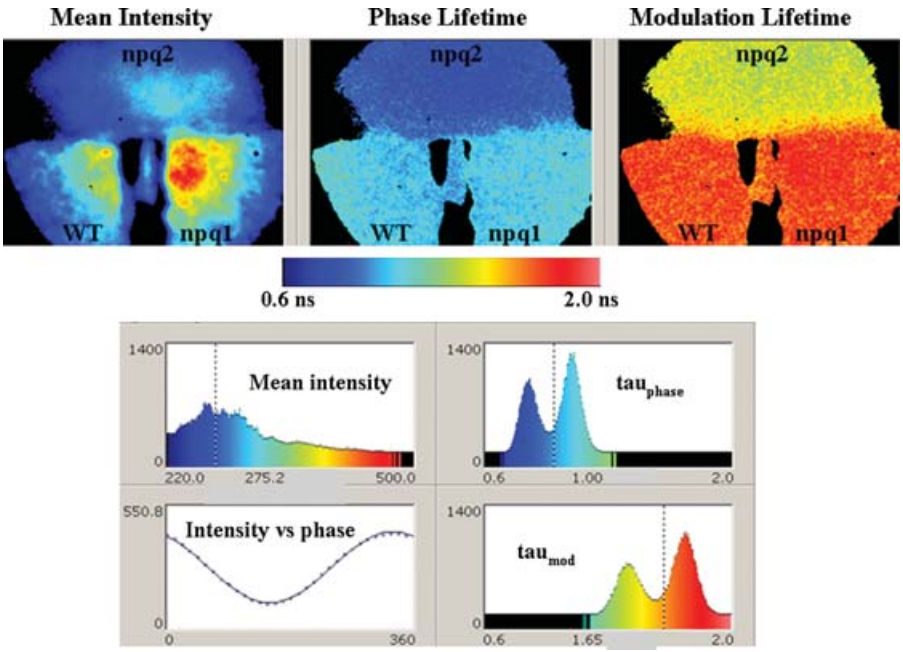

Fig. 2. Fluorescence Lifetime Imaging (FLI) images of the Chl *a* fluorescence from WT, npq1 and npq2 mutants of *Chlamydomonas reinhardtii* in a single image. Cells were immobilized on nitrocellulose filter paper. Shown are the images of the fluorescence intensity, apparent single lifetime form phase τ_{phase} and from demodulation τ_{mod}, top three panels (left to right). The mutant npq2 displays shorter intensity and τ_{phase} and values than WT/npq1. Irradiance was 2500 μmol (photons) m^{-2} s^{-1} and the total irradiation time 3.9 s. The lower panels are (clockwise from upper left): histograms of the fluorescence intensity, τ_{phase} and τ_{mod}, and an example of homodyne data averaged over pixels (sine wave) over one phase period, with the fit. The colour table corresponds to values of τ_{phase} and τ_{mod}; the same colour table is also linearly proportional to the intensity histogram.

transport from PSII to PSI (Velthuys, 1981; Wraight, 1981). The electron flow from Q_A to Q_B is halted, leaving Q_A in a reduced state. A major effect of DCMU is to increase the rate of rise from F_0 to the P level (Govindjee, 1995; Holub *et al.*, 2000). DCMU blocks electron flow, and the reactions that lead to a decay of fluorescence during the P-to-S-to-M transient (reoxidation of reduced Q_A, and lack of direct protonation from PSII due to lack of electron transport). However, DCMU allows cyclic electron transport (Joliot & Joliot, 2002; Munekage & Shikanai, 2005), and a limited extent of state transitions from state 1 to state 2, but not the reverse. Thus, a certain amount of NPQ will continue to occur even in the presence of DCMU.

Methyl viologen: Methyl viologen (also called paraquat, a bipyridinium herbicide) is one of the most efficient electron acceptors, and acts at the end of the PSI pathway (Munday & Govindjee, 1969a, b; Schansker *et al.*, 2005). It is known to lower the P-level. Reduced Q_A cannot accumulate as there is no 'blockage' of the electron flow. It is also used to study O_2-mediated damage in chloroplasts. It binds to the thylakoid membranes of chloroplasts and transfers electrons to O_2, continually forming superoxide O_2^-, which is highly damaging to the cell. The presence of O_2^- increases the level of superoxide dismutase (SOD), an enzyme that protects against reactive oxygen species. Methyl viologen usually causes a high rate of electron transport and reduces greatly the heat dissipation; that is, non-photochemical fluorescence quenching is reduced. The feedback control of carbon fixation on electron transport, present in the non-treated cells, is diminished. In the presence of methyl viologen, $NADP^+$ is not reduced, and carbon fixation does not take place.

Nigericin: The importance of the proton gradient for fluorescence quenching is well known (Govindjee & Spilotro, 2002; Finazzi *et al.*, 2003). Nigericin, a protonophore, dissipates (uncouples) the proton gradient, and has been reported to decrease (or sometimes to eliminate) the P-to-S fluorescence decline (Briantais *et al.*, 1979; Briantais *et al.*, 1980; Govindjee & Spilotro, 2002). This results in an increase of steady-state fluorescence. It is an ionophore commonly used to calibrate pH-sensitive dyes that are intracellularly trapped. Nigericin belongs to a class of ionophores that shield an ion's electric charge as it passes through the membrane, providing a polar environment for the ion and a hydrophobic face to the outside membrane. These ionophores transport a variety of ions, but these uncoupling agents specifically increase the proton permeability, as well as disconnect the electron transport chain from the formation of ATP.

Thus, nigericin has many complex and multifaceted effects, and has additional consequences other than simply dissipating the pH gradient. In spite of this complexity, we present the data on the effect of nigericin on our samples. We are aware that

an interpretation of our results in the presence of nigericin is complex; however, we consider it valuable to present the nigericin FLI results for direct comparison with untreated cells and cells treated with DCMU and methyl viologen.

3. Results and discussion

3.1. FLI images at the P-level

Chlorophyll a fluorescence intensity transients of the xanthophyll cycle mutants npq1 and npq2 and the WT (without cell walls) of *Chlamydomonas reinhardtii* have been published earlier (Govindjee & Seufferheld, 2002). The fluorescence intensities of npq2 were found to be significantly reduced (about 25–35% at the P-level) in comparison to WT and npq1, both of which showed similar results even in the presence of DCMU and nigericin. One of our goals in this study was to determine whether the reduced fluorescence intensity is due to a reduction in the quantum yield of fluorescence or whether it might originate from differences in the absorption cross sections of the fluorescent pigment beds (i.e. static quenching) e.g. by state transitions (Delosme *et al.*, 1996; Bruce & Vasilev, 2004). The following data show that changes in the fluorescence lifetimes contribute significantly to the changes in the fluorescence intensities.

3.1.1. FLI images: τ_{phase} and τ_{mod} measured at the P-level of WT, npq1 and npq2 cells. The top row of images in Fig. 2 shows the Chl *a* fluorescence intensity (left), τ_{phase} (middle) and τ_{mod} (right) images of WT, npq1 and npq2 cell ensembles (deposited on nitrocellulose filter paper). τ_{phase} and τ_{mod} were calculated from the measured phase and modulation values at the frequency of light modulation, using Eqs 4 and 5. Measurements of the three samples in Fig. 2 were obtained simultaneously in a single image. In this experiment, all the samples had the same concentration of cells before they were deposited on the filter paper, as measured by scattering at 750 nm. The scattering at 750 nm was taken as an approximate measure of the concentration of cells in WT, and npq1 and npq2 mutants. This assumes that the different mutants and treated cells scatter light equivalently at this far-red wavelength. However, the lifetime of fluorescence, as opposed to the intensity, is independent of the cellular (and Chl) concentration. This is one of the major reasons for using lifetime-resolved measurements. The symmetrical two-dimensional Gaussian excitation light was positioned centrally in each image so that each sample of filter paper was illuminated with similar excitation intensity profiles. The fluorescence intensity and lifetime images were acquired over 3.9 s during the Chl fluorescence transient. Although the excitation intensity varies over each sample, the lifetime-resolved images are homogeneous across each sample. The intensity images of the cells show 30% lower fluorescence intensity for npq2 than npq1, confirming the earlier suspension studies. WT and npq1 images show similar average intensities (WT fluorescence is only 10% less than npq1).

The decreased fluorescence intensity for npq2 is accompanied by shorter τ_{phase} and τ_{mod} values. At the light intensity (2500 μmol photons m^{-2} s^{-1}) used in this experiment, the global values of τ_{phase} and τ_{mod} (averaging the intensities over all pixels for each individual phase measurement before the phase and modulation analysis) of the WT were $\tau_{phase} = 1.11$ ns and $\tau_{mod} = 1.78$ ns. There is obviously more than one lifetime as evidenced by $\tau_{phase} < \tau_{mod}$. The measurement errors for the single pixel analysis (Fourier analysis for every pixel separately) were determined directly from the histograms and is approximately 50 ps for τ_{phase} and 70 ps for τ_{mod}. The variation errors when determining global values of τ_{phase} and τ_{mod} are less than 10 ps, due to the increase in signal-to-noise ratio by averaging many pixels (this does not mean an error in the absolute accuracy of the lifetimes). For npq1, $\tau_{phase} = 1.12$ ns and $\tau_{mod} = 1.79$ ns. These values are similar to the WT whereas npq2 displays significantly shorter values, $\tau_{phase} = 0.85$ ns and $\tau_{mod} = 1.44$ ns.

3.1.2. Two-lifetime component analysis of the FLI images measured at the P-level. The two-component lifetime analysis, as described later in Section 3.5 and Sections 3.6.1 and 3.6.2, was applied to the phase and modulation lifetime values from the data of Fig. 2 (not shown). Using this analysis, the value of the longer lifetime τ_2 for the zeaxanthin-accumulating mutant npq2 is always shorter compared to either WT or np1, and the fractional intensity of this component is also smaller, in agreement with expectations from the τ_{phase} and τ_{mod} representation (a quantitative discussion of similar data is deferred to the results and discussion of the polar plot analysis below). These results are consistent with the view that zeaxanthin quenches the Chl *a* fluorescence of PSII in *Chlamydomonas reinhardtii* by decreasing its quantum yield. This is confirmed by a reduced τ_2. τ_{phase}, τ_{mod} and the average lifetime (calculated from the two-lifetime analysis) are 20–30% shorter for npq2 compared to WT and npq1. This accounts for the 25–35% reduction in fluorescence intensity for npq2 in comparison to WT and npq1; that is, the intensity decreases proportionally to the decrease in the lifetime. Therefore, the decreased fluorescence intensity is not simply due to a decrease in concentrations of Chl in PSII (Gilmore *et al.*, 1995; Gilmore *et al.*, 1998); it is of course possible that changes in concentration also occur.

3.1.3. Treatment with DCMU, nigericin and methyl viologen. The above general conclusions apply even to cells when electron transfer is inhibited by DCMU, when the proton gradient is decreased by nigericin, and after treatment with the PSI-electron-acceptor methyl viologen (images are not shown; see P-to-S transient data below). All these results imply that the

quenching process includes contributions from non-qE related processes. However, interpreting the results is challenging. The effects of chemical treatments are complex. DCMU blocks electron flow; nevertheless, cyclic electron flow still occurs (Joliot *et al.*, 2006) and the plastoquinone pool may be reduced through chlororespiration (Bennoun, 1982). Thus, state transitions and NPQ may continue to occur (Forti *et al.*, 2006). Although nigericin decreases the proton gradient, consequently decreasing NPQ, both the state transitions and NPQ may continue to some extent. Although methyl viologen normally enhances electron flow, both NPQ and state transitions may also continue to some extent (D. Kramer, personal communication).

3.2. Fluorescence measurements during the P-to-S-to-M transient: previous measurements

The slow Chl a fluorescence transients following the 'P' (peak) level show a decrease to a semi-steady state 'S' level, sometimes followed by an increase to an 'M' (maximum) level in intact algal cells (Govindjee & Papageorgiou, 1971; Papageorgiou, 1975); see Section 1.5. Steady-state fluorescence measurements during the P-to-S-to-M transient have been used to probe several superimposed slow events in photosynthesis (Mohanty & Govindjee, 1974): (a) protonation of the thylakoid lumen (Briantais *et al.*, 1979; Briantais *et al.*, 1980), possibly leading to NPQ; (b) excitation energy transfer among PSII units and electron flow in PSII (Govindjee, 1995; Stirbet *et al.*, 1998; Steffen *et al.*, 2001); and (c) conversion of 'State 2' to 'State 1' (Allen, 2002), especially during S-to-M rise. Early reports noted the rise in fluorescence intensity at 'Hi' excitation intensities, following the initial long-time P-to-S decay (Papageorgiou & Govindjee, 1968a; Mohanty *et al.*, 1971). We have extended these studies by making lifetime-resolved fluorescence measurements during the P-to-S-to-M transient, which shall be further referred to as the P-to-S-to-M transient fluorescence lifetime measurements. Early lifetime measurements on *Chlorella* cells during the P-to-S phase have been reported (Briantais *et al.*, 1972).

3.3. The fluorescence intensities during the P-to-S-to-M transient: WT, npq1 and npq2 cells in the presence and absence of DCMU, nigericin and methyl viologen

The differences in fluorescence intensity induced by the chemical treatments that we observe when the algal cells are deposited on the filter paper (where the cells are in resting, immobile stage) are not as pronounced as reported earlier from cell suspensions (Govindjee & Seufferheld, 2002); however, we observe similar trends in our measurements of the fluorescence transients using immobilized cells.

Fluorescence intensity is automatically measured during the FLI measurement. As expected, measurements with npq2 cells always show lower fluorescence intensities (Figs 3A–D); the measured and simulated intensity curves are overlaid (see the figure legend of Fig. 3) and shorter τ_{phase} and τ_{mod} compared to WT/npq1 (direct phase and modulation data are not shown for the transient data). This is true at both the excitation intensities used. τ_{mod} and τ_{phase} are not the same (e.g. see Fig. 2), showing unequivocally the presence of multiple lifetime components. This is also a clear manifestation that τ_{phase} and τ_{mod} are not true individual lifetimes. For this reason we defer a discussion of the lifetime-resolved parameters during the P-to-S-to-M transient, as well as discussion of the simulated intensities, to Sections 3.5–3.9, where a multiple lifetime analysis is made.

In the following subsections 3.3.1–3.3.4 we summarize the intensity data during the P-to-S-to-M transient. The measured intensities can be seen in Figs 3A–D. The intensities simulated from the polar plot analysis, from Sections 3.6–3.8, are overlaid on the plots in these figures. The relative fluorescence intensities during the P-to-S-to-M transient at the two different irradiation intensities, 300 and μmol photons m^{-2} s^{-1} (identified as 'Lo'), and 2750 μmol photons m^{-2} s^{-1} (identified as 'Hi'), are shown in Figs 3A and 3B. The actual fluorescence intensity at the 'Hi' excitation intensity is about a factor 9 higher than at the 'Lo' intensity, corresponding to the difference in excitation intensity.

3.3.1. Untreated cells. Without treatment by inhibitors, the fluorescence intensity first decreases considerably during the initial phase of the P-to-S transient for WT and npq1; the decrease is less pronounced for npq2 at both intensities (Fig. 3A, top panel). At the 'Hi' excitation intensity (2750 μmol photons m^{-2} s^{-1}), the fluorescence increases after about 50 s for the WT and npq1 mutant, reaching the so-called 'M' level; such an intensity increase has been reported earlier in other algae (Mohanty & Govindjee, 1974). The S-to-M rise is absent in npq2 cells. In WT cells the P-to-S decay has been correlated with internal acidification and reoxidation of Q_A^- (Briantais *et al.*, 1979; Briantais *et al.*, 1980) and state $1 \rightarrow 2$ transition (Allen & Forsberg, 2001). The shape of the P-to-S transient depends on the level of light intensity (Fig. 3, top panel).

3.3.2. DCMU. It is well known that the rate of decrease of the P-to-S fluorescence intensity is considerably slower in the presence of DCMU. The data in Fig. 3A, bottom panels, show that the rates of the initial intensity decrease seen in the WT and npq1 cells are slower in the presence of DCMU. At the 'Lo' light level, the P-to-S transient is largely abolished in the presence of DCMU; at the 'Hi' illumination level there appears a slow decrease during the P-to-S transient. In npq2 cells, the fluorescence intensity is low and constant compared to WT/npq1 cells in 'Lo' light. In 'Hi' light, fluorescence of npq2 is relatively higher and decreases during P-to-S transient.

When the linear flow of electrons is blocked by DCMU we expect the cyclic electron flow around PSI to accumulate some protons; thus, both NPQ and state transitions may continue.

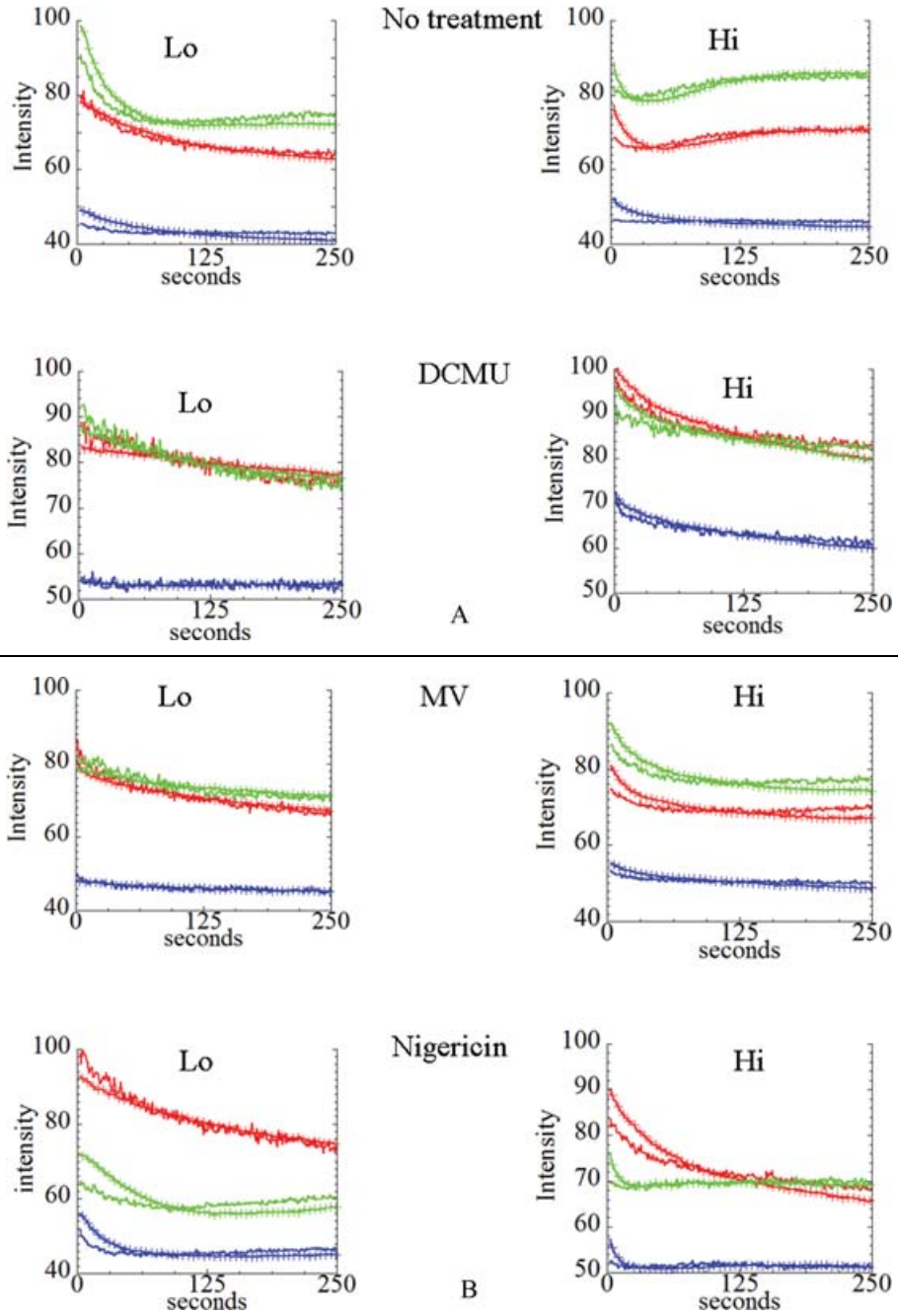

Fig. 3. Chlorophyll a fluorescence intensity transients at 300 μmol (photons) m^{-2} s^{-1}, and 2750 μmol (photons) m^{-2} s^{-1}, starting at the 'P' level. A & B: Lo = 300 μmol (photons) m^{-2} s^{-1} (A) and Hi = 2750 μmol (photons) m^{-2} s^{-1} (B). Data are shown for all treatments (see text) at both intensities. The concentrations of the inhibitors are: 10 μM DCMU, 10 μM nigericin or 100 μM methyl viologen. The number 100 on the ordinate for the intensity curves should be read as 900 when comparing data for 'Hi' intensity to those for 'Lo' intensity. In all plots, red = WT, green = npq1, and blue = npq2. The measured intensities are the smoother curves, and curves simulated from the phase and modulation analysis are the 'noisier' looking curves (see text). For clarity, the measured intensity curves are identified in A & B with '+' marks for every fourth time point. C & D: Expanded views of the 'Lo' intensity (C) and 'Hi' intensity (D) fluorescence intensity transients from Figures 3A and 3B for the untreated samples, in order to compare the details of the simulated intensity curves with the measured intensity curves. In all plots, red = WT, green = npq1, and blue = npq2. The measured intensities are the smoother curves, and curves simulated from the phase and modulation analysis are the 'noisier' looking curves (see text). Each experiment reported here was repeated at least three to five times, with consistent results.

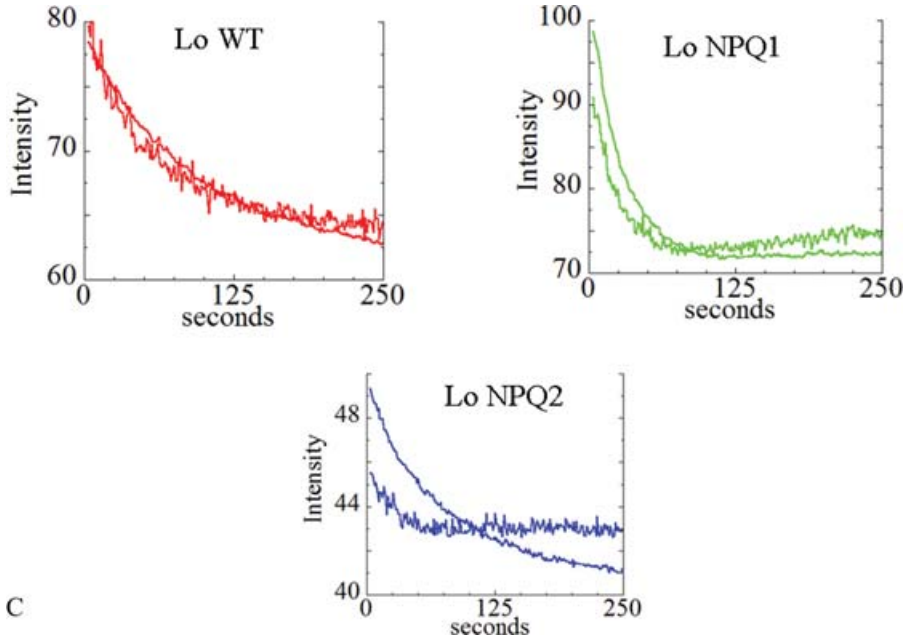

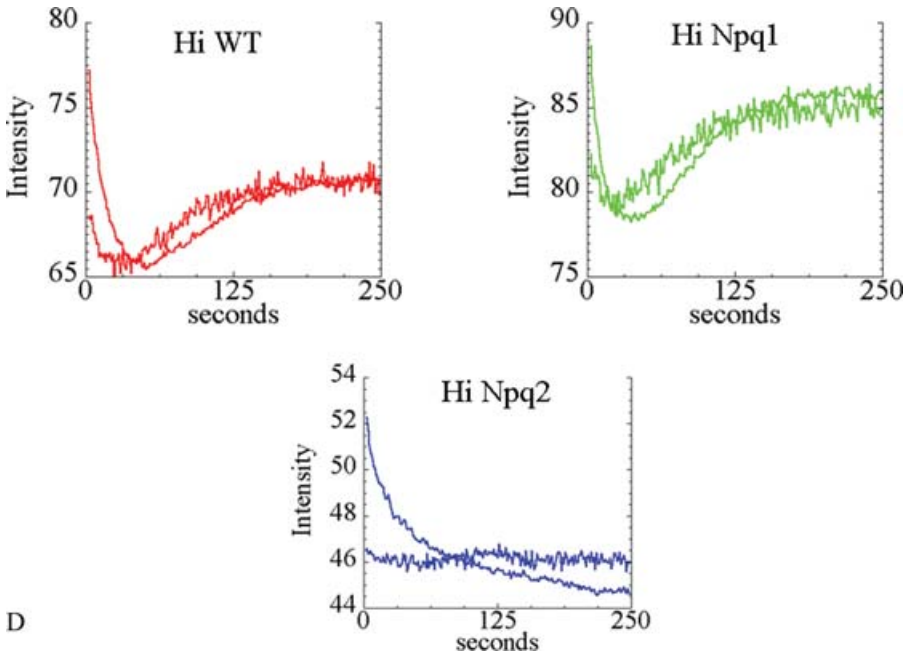

Fig. 3. Continued.

It has been shown that cyclic electron flow exists *in vivo* (Joliot *et al.*, 2006) and produces ATP (Majeran *et al.*, 2001). The decreasing intensities and lifetimes in the presence of DCMU at 'Hi' light intensity could be due to either NPQ (Gilmore *et al.*, 1998) or 'state transitions' (Forti *et al.*, 2006), or both.

3.3.3. Methyl viologen Because the P-level is reduced by methyl viologen, the fractional extent of the P-to-S fluorescence intensity is diminished. This effect can be observed clearly at 'Lo' excitation light (Fig. 3B, top left). At 'Hi' excitation light, the reduction in fluorescence at the P level is not as pronounced and the P-to-S decay is observed clearly (Fig. 3B, top right). Furthermore, methyl viologen abolished the S-to-M rise in the fluorescence intensity seen at the 'Hi' light intensity with untreated cells (Fig. 3A, top right). As we will see in Section 3.8, a major part of these changes are due to changes in quantum yields (lifetimes), and are thus related to NPQ, and are not due only to state transitions.

3.3.4. Nigericin. The Chl fluorescence intensity in the presence of nigericin (Fig. 3B, bottom panel) declines in both npq1 and npq2 cells, but after 40–50 s the intensity changes only minimally; however, the WT cells show a gradual decline in intensity. Nigericin abolished the S-to-M rise in both the WT and the npq1 cells (npq2 did not show any S-to-M rise even in the absence of nigericin (Fig. 3A, top right panel).

Nigericin had differential complex effects on the fluorescence intensity. WT increased its overall fluorescence intensity relative to npq1; however, npq2 did not change its values, which were lowest to begin with. These results suggest different ΔpH conditions of the three samples.

3.4. Heterogeneities, lifetime distributions and 'lifetime pools': interpreting the τ_{phase} and τ_{mod} during the P-to-S-to-M transient in terms of multiple lifetime components

The phase and modulation values of all data during the P-to-S-to-M transient clearly indicate more than one lifetime component (Jameson & Gratton, 1983; Clegg & Schneider, 1996) (plots of τ_{phase} and τ_{mod} for the transients are not shown). This was expected. Multiple fluorescence lifetimes have been shown for many different preparations of photosynthetic samples (Holzwarth, 1991; Gilmore, 2004; Grondelle & Gobets, 2004). Fluorescence lifetime studies on samples of membrane preparations have been interpreted in terms of lifetime distributions (Govindjee *et al.*, 1990, 1993).

In the following sections we interpret the data in terms of two (or three) lifetime component pools. Because of environmental effects (fluorophores in different molecular environments) and cell-to-cell heterogeneities, we expect a distribution of lifetimes around each major lifetime component. All emitting species will not be in identical molecular environments. We therefore speak of 'lifetime pools'; for instance, for two lifetimes (see Sections 3.5 and 3.6) we have τ_1 and τ_2 lifetime pools. The heterogeneities of intracellular environments will augment the breadth of lifetime distributions found in suspensions. In addition to these lifetime distributions (lifetime pools) about each major lifetime component, different cells will almost certainly have different fractional concentrations of fluorophores in the different lifetime pools, which will lead to cell-to-cell differences in intensity, even if distributions of lifetimes remain the same.

Heterogeneities can be more prevalent during fluorescence transient measurements, as has been emphasized (Govindjee, 1995). The measured intensity is not only a function of the quantum yield of all lifetime components, but also of the concentrations of different components of the sample, each with a different absorption coefficient. Concentrations and quantum yields can change significantly during state transitions (Allen & Forsberg, 2001), when for instance specific LHCs move from the strongly fluorescent PSII region of the photosynthetic apparatus (with longer lifetimes) to the weakly fluorescent PSI regions (Takahashi *et al.*, 2006).

In the following sections we analyze the lifetime-resolved data in terms of multiple lifetime components, assuming that the fluorescence parameters are related to a photosynthesis mechanism of an average cell.

3.5. Two-component lifetime analysis during the P-to-S-to-M transient

In order to resolve independent multiple lifetimes it would be necessary to carry out the FLI measurements at several frequencies (Weber, 1981; Jameson & Gratton, 1983; Lakowicz, 1999). We have used only a single frequency in order to achieve rapid, real-time, data acquisition during the fluorescence transients. However, if one of the lifetimes is known, it is possible to extract a second lifetime and the fractional amplitudes from the phase and modulation values at one frequency. Earlier measurements on a variety of photosynthetic preparations have shown a stable lifetime value of 0.3–0.4 ns with a substantial amplitude (Gilmore *et al.*, 1995), and a longer lifetime component of approximately 2–3 ns (Holzwarth, 1991; Gilmore *et al.*, 1995; Gilmore *et al.*, 1998). In these studies, NPQ was found to decrease the fractional intensity (or equivalently the related fractional species concentrations) of the longer component, leading to a reduction in the overall intensity.

If the phase Φ and modulation M at one frequency and the lifetime of one component τ_1 are known, the second τ_2 together with its fractional amplitude a_2 can be determined analytically for a two-component system (Weber, 1981; Jameson & Gratton, 1983; Gadella Jr *et al.*, 1993),

$$\tau_2 = \frac{\beta + \omega\tau_1}{\beta\omega^2\tau_1 - \omega}; \qquad \beta = \frac{M\cos\Phi - \left(1+\omega^2\tau_1^2\right)^{-1}}{M\sin\Phi - \omega\tau_1\left(1+\omega^2\tau_1^2\right)^{-1}}$$
$$f_2 = \frac{M\cos\Phi - \left(1+\omega^2\tau_1^2\right)^{-1}}{\left(1+\omega^2\tau_2^2\right)^{-1} - \left(1+\omega^2\tau_1^2\right)^{-1}}, \qquad (6)$$

where f_2 is the fractional contribution ($f_1 + f_2 \equiv 1$) to the steady state fluorescence intensity contributed by the second lifetime component. $f_s \equiv a_s\tau_s / \sum a_s\tau_s$, where a_s is the sth relative pre-exponential amplitude of the fluorescence decay. The above equations are analytical expressions for τ_2 and f_2. These equations can be used directly to determine the parameters of two components from single frequency data, for every time point of the transient. However, we will use a related, equivalent analysis described in Section 3.6, the 'polar plot', which provides an insightful, graphical representation of the data and an expedient method of analysis (Jameson *et al.*, 1984; Clayton *et al.*, 2004; Redford & Clegg, 2005b).

We assume a constant value of the shorter lifetime, τ_1, and we assume that this value holds globally for all data sets. We discuss below our choice for this value. For a two-lifetime component model, the intensity curve (as a function of time, t, during the transient) is related

to the lifetimes and the fractional species concentrations as:

$$\text{Intensity(t)} = C_A\left(a_1(t)\,\tau_1 + a_2(t)\,\tau_2(t)\right), \qquad (7)$$

where C_A is a constant factor (independent of time). The value of C_A is adjusted so the values of the simulated intensities can be compared on the same scale with the measured intensities. We are interested in comparing the shapes of the simulated and measured intensity curves. Therefore, we choose the value of C_A for each curve that gives the same average intensity for the measured and simulated intensity curves during the transient. In Eq. 7, we have emphasized the explicit time dependence of the variables: Intensity(t), a_1(t),$a_2(t)$ and $\tau_2(t)$. These parameters are functions of time during the P-to-S-to-M transient (the FLI data for every time point are analyzed individually). From now on, we will not explicitly indicate this time dependence. For the simulations, τ_1 and C_A are assumed constant during the transient. The fractional species populations, which change during the transient, are normalized, $a_1 + a_2 = 1$, at every time point.

3.6. *Polar plot analysis*

In order to extract multiple lifetime information throughout the P-to-S-to-M transient, we analyze the lifetime-resolved data (phase and modulation) using the 'polar plot' (Redford & Clegg, 2005b) (Sections 3.6.1 and 3.6.2, and Figs 4A and 4B). The polar plot is constructed from the measured phase ϕ and modulation M values by transforming them into the polar plot format ($M\sin\phi$ vs. $M\cos\phi$). Each point of the polar plot corresponds to one measurement of phase and modulation at a particular time during the fluorescence transient. The polar plot, and similar graphical constructions, are a standard way to display and analyze many different frequency-domain measurements, for instance dielectric dispersion (Von Hippel, 1954; Redford & Clegg, 2005b), and has more recently been used for frequency-domain fluorescence lifetime data (Clayton *et al.*, 2004; Redford & Clegg, 2005b). It provides a simple representation of the data, and provides an expedient visual overview of data that is easy to evaluate. The number of independent parameters describing a multi-component model remains the same, of course, whether one chooses to analyze the data by a polar plot or by the analytical expressions given above.

3.6.1. Basics of the polar plot analysis In a frequency domain lifetime measurement, two parameters are determined at every frequency, the phase, φ_{tot}, and the modulation, M_{tot}. The subscript 'tot' emphasizes that the measured phase and modulation values result from weighted contributions from all lifetime components. The phase and modulation are independent parameters representing the distribution of lifetimes, and they are determined separately; therefore, each parameter provides an independent depiction of the fluorescence dynamics.

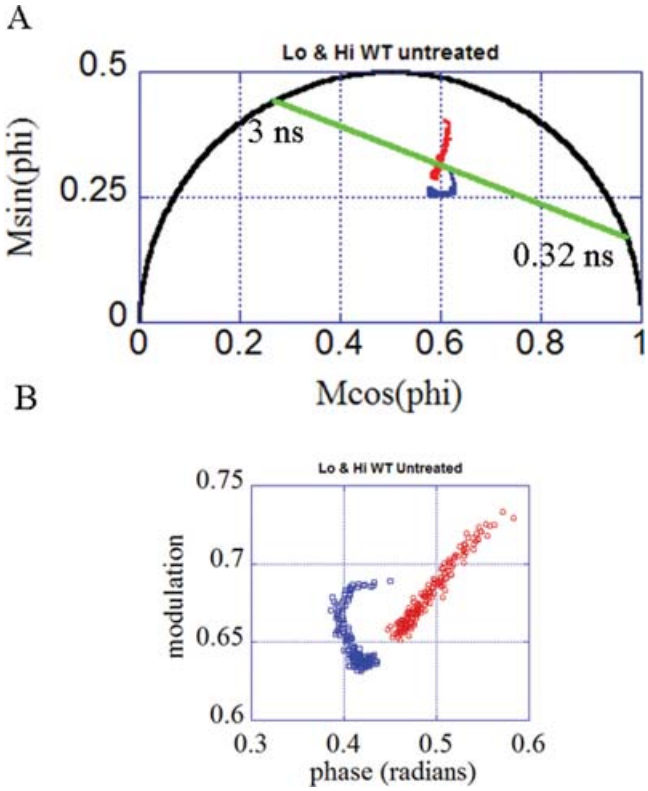

Fig. 4. Polar plot, and phase vs. modulation, of FLI data during the P-to-S-to-M transition. A. Polar plot of FLI measurements with 'Lo' = 300 μmol (photons) m^{-2} s^{-1} (red) and 'Hi' = 2750 μmol (photons) m^{-2} s^{-1} (blue) excitation intensity. The sample is WT without any treatment. The green line connects the points on the semicircle for $\tau_1 = 0.32$ ns and τ_2, passing through data points of the high- and low-intensity data. The fractional intensity for the $\tau_1 = 0.32$ ns component, f_1, is the distance on the straight line from the data point in question and the intersection of the straight line with the semicircle corresponding to τ_2, divided by the total line length from τ_1 to τ_2. The distance between the data point in question and the point on the semicircle for τ_1, divided by the total line length from τ_1 to τ_2, is the fractional intensity f_2. See text and Sections 3.6.1 and 3.6.2 for details. **B.** Plot of the modulation vs. phase with 'Lo' = 300 μmol (photons) m^{-2} s^{-1} (red) and 'Hi' = 2750 μmol (photons) m^{-2} s^{-1} (blue) excitation intensity. The sample is WT without any treatment. This plot is not as informative, or as easily interpretable, as the polar plot, but shows nicely the great difference in the transient fluorescence response of the sample to the 'Hi' and 'Lo' light intensities.

We construct a vector from the phase and modulation values in an x-y Cartesian coordinate system [with $(x, y) = (0,0)$ as the origin] such that the phase is the angle (from the x-axis) of the vector and the modulation is the length of the vector. The polar representation of this vector is:

$$x = M\cos\varphi, \quad y = M\sin\varphi. \qquad (8)$$

In this way, the combination of the phase and modulation defines a two-dimensional vector, $\vec{r}(x, y)$. In this coordinate

system, lifetime vectors (from different lifetime components) sum directly. The location of the end point of the vector is simply the weighted sum of all of the constituent locations:

$$\vec{r}_{\text{tot}} = \sum_i f_i \vec{r}_i = \int I(\tau)\vec{r}(\tau)\,\mathrm{d}\tau. \tag{9}$$

The total vector is the intensity weighted sum of the individual vectors, or the integral of a distribution, $I(\tau)$, of vectors, for all the values of the single lifetimes, τ, weighted by the fractional intensities. Here f_i is the fractional intensity of the ith single lifetime component with the phase and modulation polar vector $\vec{r}_i$. The fractional intensities are normalized such that $\sum_i f_i = 1$. $I(\tau)$ is the intensity distribution of the fluorescence lifetimes τ, where for the lifetime distribution function $\int I(\tau)d\tau = 1$. $\vec{r}_i(\tau)$ (or $\vec{r}_i$) is the phase and modulation polar vector for a distribution of lifetimes centred on τ (or τ_i). For a single lifetime component, these are defined by the equations:

$$x(\tau) = M(\tau)\cos\varphi(\tau) = \frac{M(\tau)}{\sqrt{1+\omega^2\tau^2}},$$

$$y(\tau) = M(\tau)\sin\varphi(\tau) = \frac{M(\tau)\omega\tau}{\sqrt{1+\omega^2\tau^2}}. \tag{10}$$

For a single lifetime, this representation leads to a semicircle (i.e. the point of the vector lies on the semicircle for all frequencies), where the variable is the frequency (Fig. 4).

$$y(\tau)^2 + x(\tau)^2 = M^2(\tau). \tag{11}$$

The semicircle is centred at (0.5, 0) and has a radius of 0.5. All single lifetime measurements will fall on this semicircle at any frequency. Any combination (distribution) of more than one lifetime is the weighted vector sum of the individual contributing single lifetimes in the distribution and will lie within (inside of) the semicircle. Phase and modulation combinations that lie outside the semicircle are actually physically impossible; although, in real measurements noise and other artefacts can cause data to fall there.

A two-lifetime system would have an $\frac{}{r}$ vector, which lies on the straight line intersecting the semicircle at the location of the two single lifetimes.

$$\vec{r}_{\text{tot}} = f\vec{r}_1 + (1-f)\vec{r}_2, \tag{12}$$

where f is the intensity fraction of the component #1. For the case of three components, the component lifetime vectors will form a triangle in which the total lifetime vector must lie, and so on with higher numbers of components. This model can easily be extended to the continuous case such as a Gaussian lifetime distribution (Redford & Clegg, 2005b).

3.6.2. Calculating the fractional amplitudes of two or three lifetime components and the resulting total intensity. If the measured system is composed of multiple single lifetimes, we can write the resulting vector in the polar plot as a linear combination of the single components.

$$\begin{aligned} x_i &= M_i \cdot \cos(\varphi_i), \\ \vec{r}_{\text{tot}} &= \frac{\sum_i a_i{\cdot}\tau_i \cdot \vec{r}_i}{\sum_i a_i{\cdot}\tau_i} = \sum_i f_i \cdot \vec{r}_i = \begin{bmatrix} x_{tot} \\ y_{tot} \end{bmatrix}, \quad \vec{r}_i = \begin{bmatrix} x_i \\ y_i \end{bmatrix}, \\ y_i &= M_i \cdot \sin(\varphi_i) \end{aligned} \tag{13}$$

Here a_i is proportional to the concentration of the molecular components (the pre-exponential factor), τ_i its lifetime and $\vec{r}_i$ the corresponding vector of the single lifetime component in the polar plot (the end of which lies on the universal semicircle).

The fractional intensity of a component can be written as the product of fractional concentration and its lifetime.

$$f_i = a_i \cdot \tau_i. \tag{14}$$

And we then normalize the fractional intensities as

$$\sum_i f_i = \sum_i a_i \cdot \tau_i = 1. \tag{15}$$

In the case of a three-lifetime system, we can express the resulting polar plot vector as a system of three linear equations.

$$\begin{bmatrix} x_1 & x_2 & x_3 \\ y_1 & y_2 & y_3 \\ 1 & 1 & 1 \end{bmatrix} \cdot \begin{bmatrix} f_1 \\ f_2 \\ f_3 \end{bmatrix} = \begin{bmatrix} x_{\text{tot}} \\ y_{\text{tot}} \\ 1 \end{bmatrix}$$
$$\text{with} \quad x_i = M_i \cdot \cos(\varphi_i),\ y_i = M_i \cdot \sin(\varphi_i). \tag{16}$$

This system can be solved for the fractional intensities (a_i) when the lifetimes (τ_i) of the components are known.

$$M_i = \frac{1}{\sqrt{1+(\omega\tau_i)^2}}, \quad \varphi_i = \arctan(\omega\tau_i). \tag{17}$$

To obtain the fractional concentrations we use the relation between fractional intensity with fractional concentration and lifetime:

$$a_i = \frac{f_i}{\tau_i} \cdot \frac{1}{\sum_i a_i} = \frac{f_i}{\tau_i} \cdot \frac{1}{\sum_i \frac{f_i}{\tau_i}}. \tag{18}$$

The total measured intensity expected from a lifetime system composed of these components can be calculated. This calculated intensity does not take into account instrumentation factors and must be rescaled before the comparison with measured intensities. We set the maximum intensity by multiplying by a constant, such that the average simulated intensity is equal to the average of the measured intensity, as described in the text.

$$I_{tot} = C\sum_i f_i = C\sum_i \tau_i \cdot a_i. \tag{19}$$

3.6.3. Interpreting the polar plot in terms of two lifetime components. Assuming two lifetime components with one known lifetime, the second lifetime (which varies for each time point of the fluorescence transient) can simply be read directly

from the polar plot. A straight line, starting at the location on the semicircle corresponding to τ_1 and passing through each data point of the plot, will intercept the semicircle at the point corresponding to τ_2 (Fig. 4A; see the figure legend for samples that are plotted; Fig. 4B is a plot of modulation versus phase for untreated WT at 'Lo' and 'Hi' light). The values of $f_1(t)$, $f_2(t)$ and $\tau_2(t)$ are calculated directly from the data. The fractional intensities of these two lifetime components, $f_1(t)$ and $f_2(t)$, are easily calculated from the fractional lengths of the two straight line segments between the intersections on the semicircle and the data point, as described in the Sections 3.6.1 and 3.6.2 (Redford & Clegg, 2005b). Thus, the intensity fractions $f_1(t)$and $f_2(t)$ and the second lifetime $\tau_2(t)$ can be conveniently demonstrated and analyzed graphically. The fractional concentrations of species $a_1(t)$ and $a_2(t)$are then calculated as described in Section 3.6.2.

We have shown previously that multiple distributions of lifetimes behave similarly in a polar plot analysis to multiple distinct lifetimes (Redford & Clegg, 2005b). For simplicity (and because of the complexity and heterogeneity of the photosynthetic system) we discuss the polar plots in terms of two individual lifetimes, τ_1 and τ_2 (representing two lifetime 'pools').

We assume that τ_1 (the shorter lifetime) stays constant (Gilmore *et al.*, 1998). Lifetime measurements of suspensions of chloroplasts and algae or leaves (Gilmore *et al.*, 1995; Gilmore *et al.*, 1998) have shown that NPQ leads to a decrease in the population of a slower lifetime component and an increase in a ~0.3–0.4 ns component. Different values can be chosen for this lifetime, but it is kept constant throughout all the data sets. τ_2 is the mean lifetime of the longer lifetime pool. The value for τ_2 is automatically determined for each data point during the time series once a value for τ_1 has been chosen. We describe later why we interpret changes in τ_2 to be due to a change in the distribution of τ_2 values (the analysis only finds a single value for τ_2). We have tried various τ_1 values between 0.3 and 0.4 ns for the faster lifetime corresponding to estimates in the literature of a fast lifetime component from PSII (Gilmore et al. 1995, 1998). Our interpretations are the same, regardless of the value of τ_1; for the data presented in Figs 3–5, we have assumed $\tau_1 = 0.32$ ns. Because the data must lie on a straight line passing through the measured point, and intersecting the semicircle at positions corresponding to the two individual times, longer values of τ_1 correspond to longer values of τ_2 (lever effect). We do not expect to see much contribution from PS I (which has an approximately constant lifetime value of 0.1 ns (or shorter) for Chl *a* fluorescence) (Holzwarth *et al.*, 2005). The amplitude of fluorescence from PSI is known to be very low for *Chlamydomonas reinhardtii* (Govindjee, 2004). In addition, the number of Chl molecules in PSI in *Chlamydomonas reinhardtii* is very low compared to higher plants. However, some emission from Photosystem I (Itoh & Sugiura, 2004) could be mixed into the fast component of PSII (Gilmore *et al.*, 2000).

3.6.4. Simulating the intensities from the results of the polar plot analysis. For all samples, the fractional intensity parameters f_1 and f_2 change as one progresses through the P-to-S-to-M transition. To test the goodness of the simulation, we have simulated the fluorescence intensities with the Eq. 7; the intensity fractions, f_1 and f_2, are directly proportional to the species fractions, a_1 and a_2, as $f_1 \propto a_1\tau_1$ and $f_2 \propto a_2\tau_2$. As described for Eq. 7, the simulated intensity curves have been normalized by choosing C_A so that the simulated and measured intensity curves have the same average value throughout the transient (see Figs 3A–D). The general characteristics of most curves during the P-to-S-to M transients were reproduced well by this simple two-component model.

This is not a least square regression to an analytical expression, which would result in a smooth fitted curve with no noise. And we are not smoothing the phase and modulation values in the slow transition curves before making the polar plots and simulating the intensities. Thus, when the intensities are simulated from the phase and modulation data, the random deviations are larger for the simulations than for the directly acquired intensity data. As mentioned above, we are primarily interested in comparing the shapes of the simulated transition curves.

3.7. General characteristics and interpretation of the P-to-S-to-M transient in terms of an exchange between two-component lifetime pools

Before progressing to specifics of the lifetime-resolved experiments, we point out a general feature of our interpretation. For most samples, τ_2 increases (Figs 5A and C), and the species fraction of the slow component (a_2) decreases (Figs 5B and D), as the transient is traversed; simultaneously, the species fraction of the faster component (a_1) must increase. This behaviour is seen for all samples except the 'Hi' intensity experiments without inhibitors for WT and npq1.

At first sight, it may seem inconsistent that τ_2 increases with the decreasing overall fluorescence intensity. However, a_2 decreases, and this leads to a decrease in the intensity of the τ_2 component. An increasing value of τ_2 with a concomitant decreasing intensity is explicable if there is a distribution of fluorophores with lifetime values centred on τ_2. During the P-to-S transient, a fraction of molecules in the τ_2 pool pass to the τ_1 pool, decreasing a_2. The increasing value of τ_2 during the P-to-S transition indicates that those molecules exhibiting faster τ_2 values transfer to the τ_1 pool more readily that those molecules with slower τ_2 values. Perhaps the Chl *a* molecules with faster τ_2 values are already closer to the molecular environment that exhibits partial quenching before they are eventually transferred to the τ_1 pool.

If there were a gradually varying dynamic quenching event acting on the τ_2 species, for instance due to dynamic Stern-Volmer quenching or FRET by bringing Chl molecules progressively closer to an acceptor (such as the zeaxanthin),

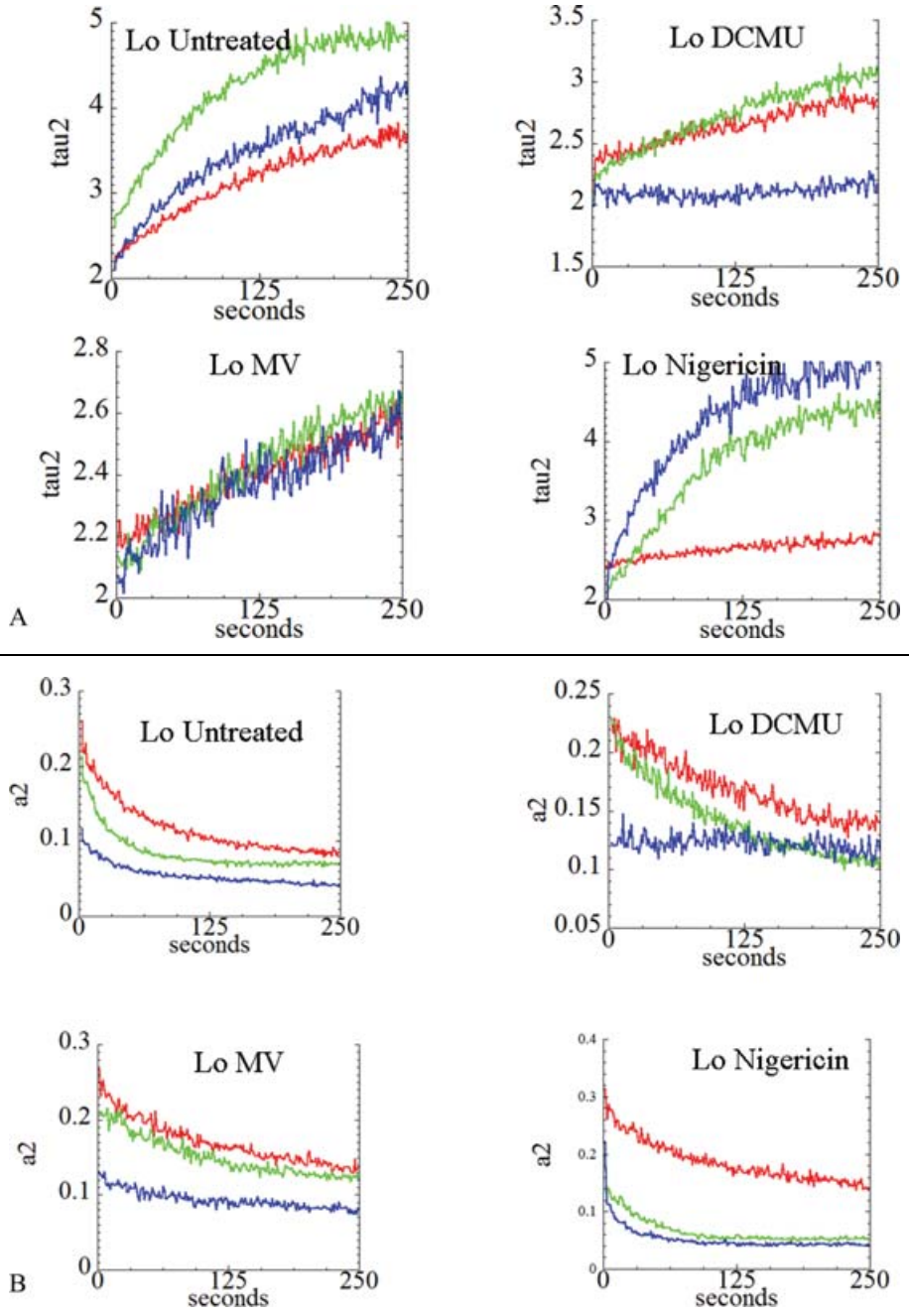

Fig. 5. τ_2 and a $_2$ values during the P-to-S-to-M transient. Data are shown for 'Lo' light intensity conditions [A (τ_2 values) and B (a_2 values)], and for 'Hi' intensity conditions **C** (τ_2 values) and **D** (a_2 values). Data are shown for untreated cells, and cells treated with DCMU, nigericin and methyl viologen. The parameter values, which are plotted vs. time during the P-to-S-to-M transient, are derived from an analysis of the polar plots for each sample. See text for details and discussion. The colour code is identical to that in Fig. 3.

this would result in a gradually increasing degree of dynamic quenching (gradual decrease in τ_2) as the P-to-S transition is traversed. This is not observed. Rather, it seems there is a transfer of molecules from an environment with relatively little quenching, within the τ_2 lifetime pool, to an environment with significantly more quenching, within the τ_1 lifetime pool. We do not imply that there is a large physical movement (such as during state transitions). The molecules change from a state with little quenching to a state with much greater quenching, and this takes place in a single step. Thereby the population of the τ_2 lifetime pool decreases and that of the τ_1 lifetime pool increases. This interpretation is consistent with all the

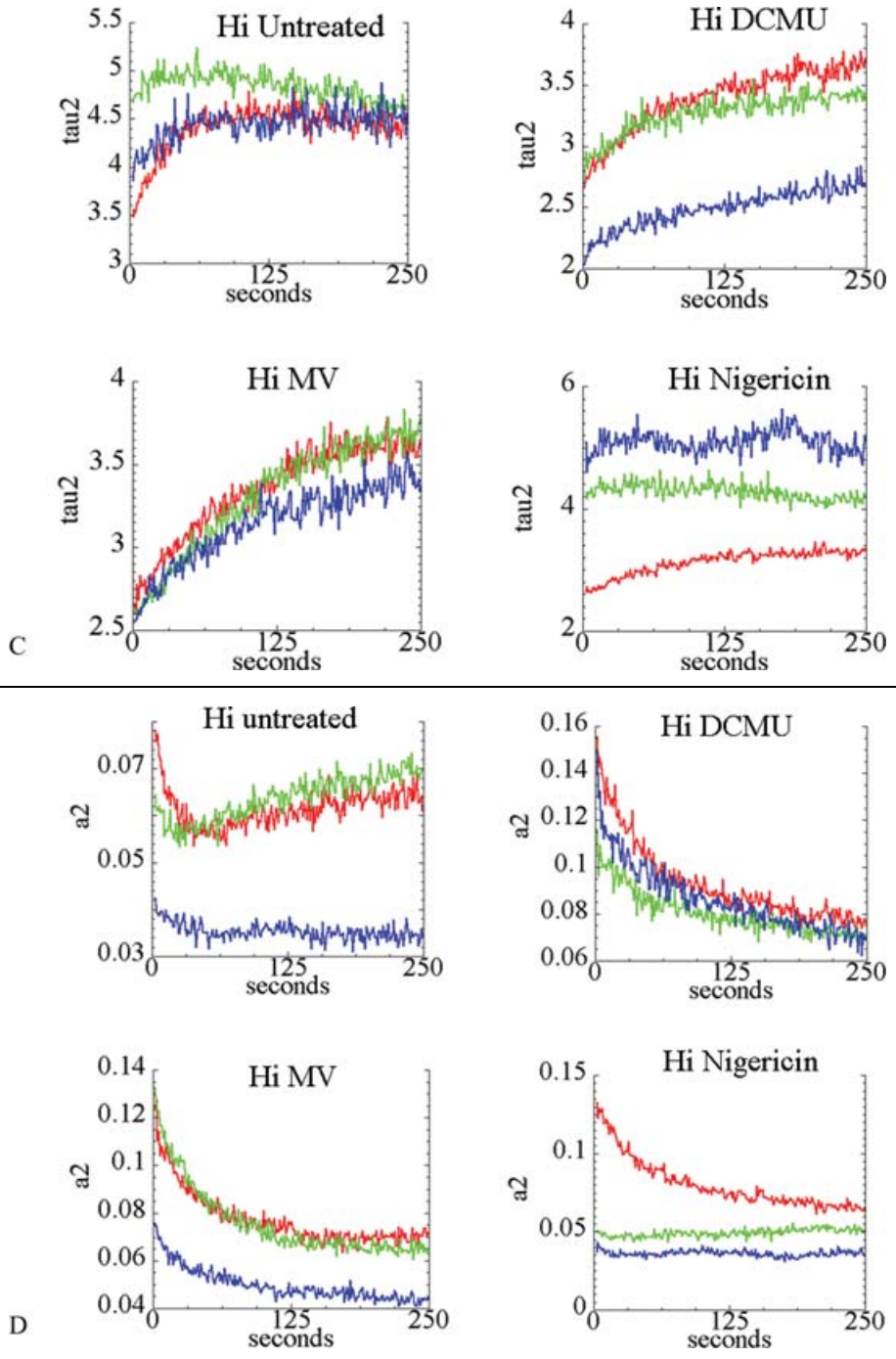

Fig. 5. Continued.

data with WT, npq1 and npq2, as well as the experiments with and without the inhibitors. It is also in agreement with the existence of a '*dimmer*' switch for photoprotection (Govindjee, 2004).

Incidentally, increasing values of τ_2 show that we are not observing simple photolytic destruction of the fluorescent molecules; otherwise, those molecules with longer values of τ_2 would tend to undergo photolytic damage first, and this would statistically lead to a reduction of the observed τ_2 under continual illumination. It seems that the observed quenching (decreasing intensity) is related to the particular spatial distribution of the fluorescent molecules; those molecules with shorter τ_2 values are already located such that they can more readily become maximally quenched and join the τ_1 pool (as

though they were already partially dynamically quenched, *e.g. via* FRET).

We now consider the lifetime-resolved data for WT, npq1 and npq2 cells, and the effects of DCMU, nigericin and methyl viologen in light of this interpretation, assuming two pools of molecules with different lifetimes and a distribution of τ_2 lifetimes.

3.8. Specific results of the WT, npq1 and npq2 cells with and without DCMU, nigericin and methyl viologen: two lifetime component pools

The experiments were carried out at two levels of illumination (300 and 2750 μmol photons m^{-2} s^{-1}); as mentioned above, we refer to these two intensities as 'Lo', and 'Hi'. As is well known, the level of illumination significantly affects the character and shape of the P-to-S-to M curves (Papageorgiou, 1975).

Kinetic processes and biological interactions in live, functional cells, such as the green alga *Chlamydomonas reinhardtii*, are numerous, diverse and complex (Rochaix *et al.*, 1998; Larkum *et al.*, 2003). Our goal is not to identify and analyze every individual fluorescence component during the transient curves. Our goal is to use the lifetime-resolved data to ascertain major features of the underlying mechanisms. Even with this simple two-component model for interpreting the lifetime-resolved fluorescence data, which also assumes that we are observing only fluorescence from PS II, it is possible to account for the P-to-S-to M transitions remarkably well. We have organized below the data into four groups: no inhibitors, DCMU, methyl viologen and nigericin.

3.8.1. No inhibitors – WT, npq1, npq2

3.8.1.1. 'Lo' excitation intensity (300 μmol photons m^{-2} s^{-1}), no inhibitors. In all cases at 'Lo' excitation intensity, τ_2 increases during the time course of the P-to-S transient (Fig. 5A, top left panel). The value a_2 decreases during the slow transient (Fig. 5B, top left panel) and accordingly a_1 increases (not shown). The intensities simulated from the lifetime data overlay the measured intensities in Figs 3A–D. The measured and simulated intensity transients agree reasonably well for the WT and npq1 cells (Fig. 3A, top panel). For the npq2 cells, the kinetic progression of the measured intensity transient is not well represented by the simple two-lifetime model, at least at this level of analysis (Fig. 3C, lower panel). The continual decrease in the measured intensity of npq2 is not present in the intensity curve simulated from the lifetime-resolved data. This is indicative of a slow kinetic process, which is not represented in the lifetime-resolved parameters. For instance, this would be consistent with a state transition. A state transition would not change the lifetimes of the fluorescent Chl molecules of PSII (which are assumed to be in the τ_1 and τ_2 pools), but would decrease the intensity of the PSII fluorescence by transferring some of the antenna Chl complexes (CP26, CP29 or a specific LHCII) from the PSII to the PSI region. If these antenna molecules were simply to become free, we would expect a higher fluorescence intensity originating from those Chl molecules in free LHCs, where they cannot transfer their energy.

The measured intensity for the npq2 cells (Fig. 3A, top left panel) and values of a_2 (Fig. 5B, top left panel) are considerably lower than for the WT and the npq1 cells. The rapid decay of the simulated intensity for npq2 arises from the rapid decrease in a_2 (Fig. 3C, bottom panel). This behaviour is probably due to the pool of readily available zeaxanthin in npq2, which does not require any time delay to affect the extent of quenching. The longer τ_2 values for npq2 (Fig. 5A, top left) compared to WT may indicate efficient quenching of the faster portion of the τ_2 pool chromophores by zeaxanthin (always present in npq2), which removes those molecules from the τ_2 pool with faster lifetimes to the τ_1 pool, even before illumination (according to the model discussed in Section 3.7). This may imply that the qT component of the P-to-S decay is more prevalent in the WT and npq1 cells, whereas the qE component is more prevalent in the npq2 cells.

The longer value of τ_2 for npq1 compared to WT or npq2 (Fig. 5A top left) is reasonable considering the lack of zeaxanthin in this mutant, and its inability to produce zeaxanthin due to the lack of violaxanthin de-epoxidase activity. This could mean that the molecular environment of many Chl molecules in npq1 does not lead to as much partial quenching as in WT and especially as in npq2 (related to the lack of zeaxanthin), thereby skewing the τ_2 distribution to longer values than for WT or npq2.

3.8.1.2. 'Hi' excitation intensity (2750 μmol photons m^{-2} s^{-1}), no inhibitors. At 'Hi' excitation light, the progress of the slow (0–250 s) fluorescence transient curves for the WT and npq1 (Fig. 3A, top right panel) are quite different from the corresponding 'Lo' excitation intensity curves (Fig. 3A, top left panel). The major distinctive characteristic at 'Hi' illumination, clearly apparent in WT and npq1 cells (Fig. 3 D), is an increase of fluorescence intensity following a minimum at about 50 s (the S level). This dip and the increase of fluorescence intensity (to the M level) are well represented by our kinetic simulations, indicating that the simple two-lifetime model captures the major underlying kinetic processes. This behaviour of the intensity for WT and npq1 fluorescence could include an initial state 1 to state 2 transition and then its reversal to state 1 (state transitions), although at normal light intensities this usually takes place slowly. Alternatively, initial rapid quenching by NPQ *via* zeathanthin could be present, followed by its reversal. At any rate, the values of a_2 (Fig. 5D, top left) show an exchange of fluorescent molecules from the τ_2 pool to the τ_1 pool, and then back to the τ_2 pool.

As expected, the fluorescence intensity for npq2 is considerably lower than for npq1 or WT (Fig. 3A, top right

panel). The npq2 mutant does not exhibit the reversal of quenching (i.e. the SM rise; Fig. 3D bottom panel) seen for WT and npq1 (Fig. 3D, top panels), and the intensity decreases continually, in contrast to the simulated intensity (similar to the behaviour at 'Lo' intensity (Fig. 3C bottom panel). The value a_2 (Fig. 5D upper left) decreases rapidly to a plateau for npq2.

Again, similar to the 'Lo' illumination intensity (Fig. 3C), the fluorescence intensity curve for npq2 is not well represented by the simple two-lifetime model (Fig. 3D). The simulation from the phase and modulation data predicts a decrease in intensity, in contrast to the measured intensity. At these 'Hi' light intensities, the value of a_2 for the npq2 mutant is essentially constant over time (Fig. 5D top left), in contrast to the same parameter for WT and npq1.

As for the 'Lo' intensity data, the striking difference between the measured and simulated intensity curves for npq2 is consistent with the conversion of some fluorescent Chl-protein complexes to complexes that do not contribute (either directly or indirectly) to observable changes in the fluorescence lifetime parameters. Whatever the mechanism, it is probably related to the permanent availability of zeaxanthin in npq2, which is evident from the low values of the measured intensity. The value a_2 for npq2 is also considerably lower than for WT or npq1 (Fig. 5D), and in agreement with the intensity, a_2 shows the absence of the S-to-M fluorescence rise in npq2. The rise in S-to-M fluorescence, present in WT and npq1 mutant at 'Hi' intensity (Fig. 3A), and observable in the rise in a_2 (Fig. 5D left panel), is somehow mechanistically blocked in the npq2 mutant. As for the 'Lo' intensity curves, at 'Hi' intensity τ_2 for npq1 is somewhat longer than even for the WT (Fig. 5C), and this is further indication of the lack of zeaxanthin. Further experimentation is required to quantitatively identify and separate the physical basis of the different quenching processes.

In general, the underlying kinetic processes appear to take place more rapidly under the 'Hi' intensity conditions than under the 'Lo' intensities, as one would expect. For WT, the long time increase in a_2 acts synergistically with a constantly increasing value of τ_2(approaching a constant plateau). For npq1 the increasing intensity is due solely to an increase in a_2 (Fig. 5D), since τ_2 actually decreases over this part of the transient (Fig. 5C).

The opposing progression of a_1 and a_2 during the transient is consistent with the idea of a 'dimmer switch' (Gilmore & Govindjee, 1999). Of course, this behaviour is inherent in our lifetime-resolved model, because we have assumed only two lifetime component pools. Therefore, if the fractional species a_2 increases, a_1 must decrease. Thus, during the slow transient at 'Lo' excitation intensity, fluorescent molecules in the longer lifetime pool (higher intensity per molecule) are 'switched' to the shorter lifetime pool (lower intensity per molecule). At 'Hi' light intensity there is a reversal of the 'dimmer switch' (Fig. 3D) for WT and npq1.

3.8.2. DCMU. The behaviour during the P-to-S transient in the presence of DCMU is radically different from the untreated samples.

Two striking observations of the DCMU data are: (1) There is no S-to-M fluorescence rise, beginning at ~50 s (Fig. 3A bottom panel) as was observed in the transient for WT and npq1 at 'Hi' illumination intensity (Fig. 3A top panel). This may imply that the SM transient reflects a transient reduction of Q_A, which DCMU abolishes. (2) The values of the fluorescence intensity, a_2 and τ_2 are constant over the P-to-S transient for npq2 at 'Lo' excitation intensity (Figs 5A and B). Changes in the intensity, a_2 and τ_2 for WT and npq1 at 'Hi' excitation intensity are gradual compared to the untreated samples (Figs 5C and D). The intensity for npq2 is again lower than for WT and npq1, for both 'Hi' and 'Lo' light intensities, even in the presence of DCMU; this is also true for a_2. This is an indication that quenching by zeathanthin functions even when the linear electron flow is blocked by DCMU. This is perhaps due to cyclic electron flow around PSI, which as discussed earlier, is known for some systems to occur (Joliot *et al.*, 2006). This may contribute sufficiently to the change in pH for efficient quenching by NPQ to function.

The lower fluorescence intensity of npq2 compared to WT and npq1 is less pronounced at 'Hi' than at 'Lo' light intensity (Fig. 3A, lower panels). Since DCMU partially mimics 'Hi' light intensity, in that Q_A is reduced to a greater extent in both cases, this is perhaps to be expected. However, the mechanism responsible for the delayed rise in the fluorescence (S-to-M transient), seen for untreated WT and npq1 (Fig. 3A right panel, and Fig. 3D), is apparently blocked by DCMU. Perhaps a functioning electron flow through PSII is necessary for the S-to-M rise in fluorescence. By contrast to 'Lo' excitation intensity, changes in fluorescence intensity, a_2 and τ_2 are observed for npq2 at 'Hi' intensity (Figs 3A and 5C and 5D); τ_2 is considerably shorter for npq2 than for WT and npq1 mutant (Fig. 5C, upper right).

The simple two-lifetime model accounts well for the measured fluorescence intensities even for npq2 (Fig. 3A, bottom panel) which emphasizes the excellent correspondence between the lifetime-resolved measurements and the steady-state intensity data using this simple two-component model in the presence of DCMU. This indicates that we are observing the major kinetic phenomena with the two-component lifetime-resolved analysis in the presence of DCMU. For instance, the deviation between the measured and simulated intensities for the untreated npq2 cells (Fig. 3C, lower panel) at 'Lo' light is not observed in the presence of DCMU (Fig. 3A, lower left).

At both 'Lo' and 'Hi' light intensity, we again observe a behaviour consistent with the idea of a 'dimmer switch', but less pronounced than in the absence of DCMU.

Further, we observe for both 'Lo' (Fig. 5A) and 'Hi' (Fig. 5C) illumination conditions that τ_2 increases during the transient for WT and npq1; therefore, for these samples in the presence of DCMU the decreasing fluorescence intensity

is due to decreasing values of a_2, not to a decreasing τ_2. Our interpretation is the same as for untreated cells; that is, there is an exchange of molecules in the τ_2 pool into the τ_1 pool. Apparently, Chl molecules in the τ_2 pool with shorter τ_2 values become quenched (join the τ_1 pool) more readily than those with longer τ_2 values, also in the presence of DCMU.

3.8.3. Methyl viologen. Interestingly, at both 'Lo' and 'Hi' light intensities, methyl viologen appears to induce WT and npq1 to react almost identically (referring to intensity, τ_2 and a_2) during the P-to-S transient (Fig. 3B, top panel, and Figs 5A–D), whereas npq2 behaves differently. This is to be contrasted with nigericin, which induces npq1 and npq2 to behave similarly. Although both npq2 and npq1 have a dysfunctional xanthophyll cycle, npq2 has a large permanent concentration of zeaxanthin, and npq1 has none; however, WT has relatively low concentrations of zeaxanthin after dark adaptation. Methyl viologen pulls the photosynthetic system rapidly through to the end of PSI, and is expected to reduce considerably the extent of NPQ reactions in WT.

The lower value of a_2 for npq2 than for WT and npq1 in the presence of methyl viologen (Figs 5B and D) (as well as the lower measured intensity (Fig. 3B) is probably due to the permanent presence of larger amounts of zeaxanthin, which is missing in npq1 and low in resting WT.

The fluorescence intensity curves (Fig. 3B, top panel) during the time course of the transient proceed with similar shapes for WT, npq1 and npq2 cells, with the intensity of npq2 being lower, as expected. This is probably because methyl viologen effectively pulls the total reaction through to the end, not giving intermediates an opportunity to accumulate to the normal extent. At 'Lo' intensity, the τ_2 values in the presence of methyl viologen are essentially identical for WT, npq1 and npq2 throughout the whole P-to-S transient (Fig. 5A, bottom left); they all increase only slightly and gradually. At 'Hi' intensity, the τ_2 values of WT and npq1 both increase identically (Fig. 5C, lower left) and begin with similar values as at 'Lo' intensity. The τ_2 values for npq2 are slightly lower than for WT and npq1, and the increase during the P-to-S transient is somewhat less. The rate of increase in τ_2 is markedly less for the methyl viologen treated cells than for untreated WT, npq1 and npq2 cells.

The value of a_2 decreases as the transient is traversed in all samples with methyl viologen (i.e. the proposed 'dimmer switch' is still active) (Figs 5B and D, lower left). At 'Lo' and 'Hi' light the shapes of the simulated intensities match well with the measured intensities (Fig. 3B, upper panel). In general, in the presence of methyl viologen the lifetime-resolved analysis with just two lifetime pools captures the major features of the long time transient.

3.8.4. Nigericin. As mentioned in the Materials and Methods, nigericin produces many changes that affect the physiology of the cells at multiple points in the photosynthetic mechanism. Therefore, the discussion below is mainly descriptive, and the interpretations are speculative. Clearly, these observations require further study in order to understand the mechanistic implications.

NPQ is expected to be strongly inhibited in plants treated with nigericin, because a proton gradient across the thylakoid membrane is necessary for the operation of the xanthophyll cycle leading to NPQ. A striking aspect of our FLI data in the presence of nigericin is that npq1 and npq2 react almost identically at 'Lo' (Figs 3B and 5A and B) and 'Hi' (Figs 3B and 5C and D) light intensity, but are very different from the WT cells. Also, the lifetime-simulated intensities with two components capture well the major features of the measured intensities for all cases with nigericin. The S-to-M rise of fluorescence intensity (and corresponding values for a_2) beyond 50 s, seen in the untreated WT and npq1 cells, is eliminated in the presence of nigericin (Figs 3B and 5D). Interestingly, at 'Lo' intensity there is a weak rise in fluorescence at longer times for npq1 and npq2 in the intensities simulated from the lifetime analysis. For the untreated cells, this rise is only found at 'Hi' light intensity (albeit much more pronounced). For npq1 and npq2, the initial decrease in fluorescence intensity, concomitant with a rapid decrease in a_2, is much faster than in WT. For npq1 and npq2, these changes are largely completed after about 40 s at 'Lo' light intensity (Fig. 5B right) and they are almost instantaneous at 'Hi' light intensity (Fig. 5D, right). For WT, the monotonic changes in these parameters occur over the entire time range of 250 s. At 'Lo' intensity, the fraction a_2 for WT is more than double the value of a_2 for npq1 and npq2, and this is also approximately true at 'Hi' light (Figs 5B and D). Also at 'Lo' light, τ_2 hardly rises during the transient for WT (Fig. 5A); it starts at almost the same value as both npq1 and npq2. By contrast, at 'Lo' light τ_2 increases considerably for npq1 and npq2 during the transient, and continues to rise much longer than the changes in either a_1 or a_2.

It is not clear why nigericin causes npq1 and npq2 to react similarly during the transient (for the fluorescence intensity, as well as τ_2 and a_2) and their behaviours are very different from the WT result. Perhaps this is related to the fact that in both mutants the xanthophyll cycle is not operative. The operation of the xanthophyll cycle requires the pH gradient, which is abolished by nigericin. Without nigericin the xanthophyll cycle is still operative in the WT, but not in npq1 and npq2. Perhaps the elimination of a functioning pH gradient in the presence of nigericin, in conjunction with the lack of a functioning xanthophyll cycle (npq1 and npq2), is necessary to greatly diminish the P-to-S transient. In this respect, it is interesting that in the presence of nigericin and 'Hi' light intensity the P-to-S transient is absent for npq1 and npq2, in contrast to the response of WT. Further, τ_2 for both mutants does not change with time at 'Hi' light intensity (Fig. 5D, bottom right), as expected from the very rapid intensity changes. The continually decreasing intensity for WT, and the corresponding a_2 curve for the WT, may be due to

another mechanism besides a functioning NPQ contributing to the proposed 'dimmer switch'.

3.9. Interpreting the polar plot in terms of three constant lifetime components

A three-lifetime model involves an exchange between individual pools of Chl species with different, but constant, lifetimes. By 'exchange' we do not mean a physical movement, but exchange of molecules between pools of molecules defined only by their lifetimes. Two lifetimes cannot describe the data if both lifetimes are kept constant. To test whether a model with three constant lifetimes can account for the general characteristics of the data, we have analyzed the polar plot data in terms of three constant lifetimes, and extracted the component intensity fractions as discussed in Sections 3.6.1 and 3.6.2. We choose 0.32 ns for the shortest time (Gilmore *et al.*, 1995; Gilmore *et al.*, 1998). For this analysis, two slower lifetimes were chosen, which remain constant throughout the P-to-S transition. The fractional intensities were extracted from the individual data points on the polar plot of the P-to-S transition, and the overall fluorescence intensity during the P-to-S transient was then compared with the measured intensity (Sections 3.6.1 and 3.6.2). We found an increase in the fraction of the fast species, and a decrease in one of the slower components whereas the other slower component increased (data not shown). The concentration of the slowest component that increases is relatively low. We have carried out this analysis for all the data: WT, npq1 and npq2, with and without DMCU, nigericin and methyl viologen. We assume global values of all the three lifetimes (that is, the same for all samples); of course, there is no guarantee that the lifetime values should be the same for all cases, but this is the simplest model. The underlying lifetimes and distributions are probably somewhat different for each cell type and for the different inhibitors.

The three constant-lifetime model accounts for the intensity data in a similar way as the simpler two-lifetime model (data not shown). However, rather than changing the longer lifetime continuously during the P-to-S transient, there is a trading of fractional species concentrations between the two longer lifetime species, as well as a decrease of the fractional species of the shorter of the two long lifetimes during the transient, leading to an increase in the species concentration of the τ_1 pool (data not shown). The fractional intensity of the slowest time usually increases during the transient. This corresponds to the increase of τ_2 in the two-lifetime model. The overall interpretation in terms of three constant lifetimes is similar to that of the two lifetimes with only one lifetime able to vary.

3.10. Heterogeneities of fluorescence parameters in different cells, and within cells, which affect lifetime pools

We have interpreted changes in τ_2 from FLI measurements during the P-to-S-to-M transient in terms of lifetime pools with distributions around central lifetime values. Lifetime distributions within each observed lifetime pool could have several origins: (1) distributions inherent in the photosynthesis mechanism in each cell (this is the assumption of our interpretations); (2) the cells within an ensemble probably exist in somewhat different physiological states (especially related to their dynamic response to light) and (3) different locations in individual cells may exhibit different lifetime characteristics. We carried out series of FLI experiments on cells to explore these possibilities. In all our FLI measurements during the PSMT transient it was necessary to check whether the cells mostly showed homogeneous lifetimes. If significant differences in lifetimes were present between cells, it would have added artefacts to our lifetime analysis. The imaging experiments also showed the necessity of care and reproducibility in the preparation of the samples.

3.10.1. Comparison of swimming and resting cells: fluorescence changes. Cells kept under motion, with high mobility (see Materials and Methods), were compared with resting (motionless) cells (Fig. 6). Cells left for 1–2 h in a capillary tube in the dark reduce their mobility and tend to accumulate at the top of the tube, which has been referred to as negative geotaxis (Bean, 1977; Fornshell, 1978; Bean, 1984; Harris, 1989). Resting *Chlamydomonas* cells after being in the dark for extended periods have decreased photosynthetic activity, and they lose their variable Chl fluorescence (Govindjee and Reto Strasser, unpublished observations).

Under constant illumination, cells filled in micro-capillaries (see Material and Methods) did not stop moving even after 24 h. In darkness, the cells first showed a 'shaking' movement, moving only slightly about their centres. Some cells rotated, showing movement of only one flagellum. About 70% showed negative geotaxis and 30% showed positive geotaxis. After 2–5 h in the dark, all cells stopped swimming, shaking or rotating. Fig. 6A shows WT, npq1 and npq2 cells in micro-capillaries, directly after filling the cells into the capillary (swimming cells; top panels) and after 2 h in the dark (resting cells; Fig. 6B). The values τ_{phase} and τ_{mod} of the npq2 swimming cells are 20% shorter than the lifetimes of the WT/npq1 swimming samples (Fig. 6A) in agreement with the results presented above.

The resting cells (Fig. 6B) have reduced fluorescence intensities and reduced phase and modulation lifetimes. The fluorescence intensities for the WT and npq1 samples are reduced compared to the swimming cells by over 40%; τ_{phase} is reduced by 70% and τ_{mod} is reduced by 30%. On the other hand, npq2 shows only a 10% reduction in both the intensity and τ_{phase} compared to swimming cells. Interestingly, in this case npq2 has even longer lifetimes than WT/npq1.

We conclude that both Chl *a* fluorescence intensities and lifetimes of *Chlamydomonas reinhardtii* depend on the physiological state of the cells. The precise physiological state of swimming or darkness-induced resting cells is unknown. Several factors are involved (Harris, 1989) : (1) negative

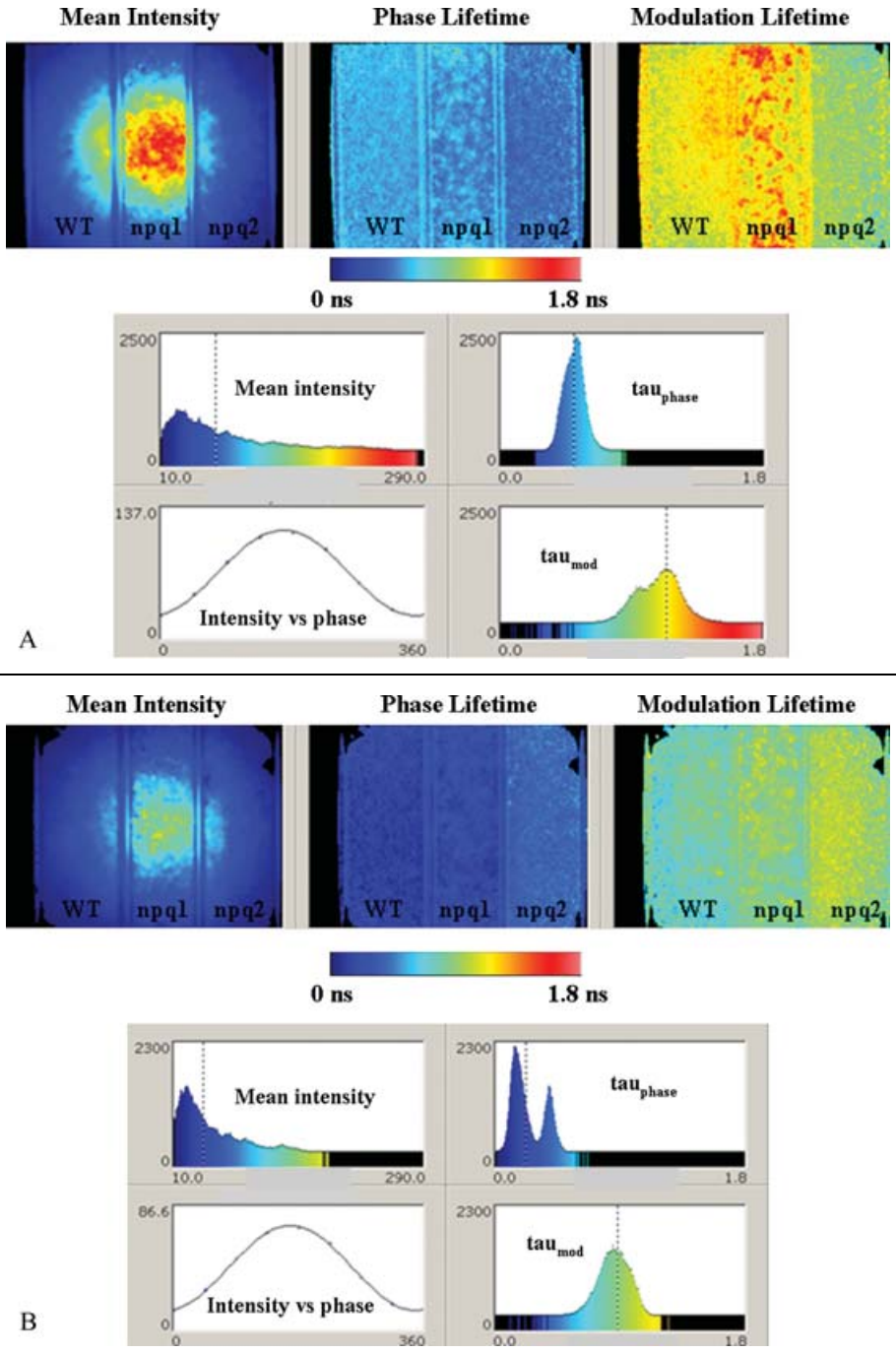

Fig. 6. Comparison of chlorophyll fluorescence in swimming and resting cells of *Chlamydomonas.* Signals from ensembles of cells of WT, npq1 and npq2 mutants of *Chlamydomonas reinhardtii* in micro-capillaries. Irradiance, 1400 μmol (photons) m^{-2} s^{-1}. A) Top panels: swimming cells directly after filling the capillaries. Top three panels show, from left to right: fluorescence intensity, τ_{phase} and τ_{mod} images. The bottom four panels are (clockwise, starting from upper left): histograms of the intensity image, and the τ_{phase} and τ_{mod} images, and an example of the homodyne sine wave data averaged over selected pixels together with the fit. B) The same sample as in A, after 2 h in the dark (resting cells). Top three panels show, from left to right: intensity, τ_{phase} and τ_{mod} images. The bottom four panels are (clockwise, starting from upper left): histograms of the fluorescence intensity image, and the τ_{phase} and τ_{mod} images, and an example of the homodyne sine wave data averaged over selected pixels together with the fit. In the resting state, the cells display reduced intensities and lifetimes.

geotaxis; (2) cell cycle, regulated by biological timers (Donnan & John, 1983); (3) changes in cell division and (4) most importantly, differences in the bioenergetics, for example, swimming cells use ATP for motion, whereas in resting state, many biochemical reactions are not active. The cell cycle of *Chlamydomonas* seems to be regulated by what has been called an 'hourglass' category of biological timers (Donnan & John, 1983; Harris, 1989). Light and dark periods function as a stimulus for cell division commitment points and the cell cycle is regulated by photosynthetic activity. If one is subjecting a light-grown culture to overnight darkness, one will get small cells of identical size on the next day (Harris, 1989). These effects could undoubtedly contribute to heterogeneities and lifetime distributions in cellular populations, affecting any measurement of fluorescence lifetimes as well as intensities. These results stress the importance of adhering to a strict routine when preparing the samples for the FLI measurements, as we have done.

3.10.2. Fluorescence lifetime images of single cells: Lifetime heterogeneity between and on single chloroplasts

3.10.2.1. τ_{phase} and τ_{mod} values are usually homogeneous within each cell, but can change over time. FLI measurements of single cells immobilized on a thin film of agar were carried out. Five minutes of dark adaptation before each measurement was allowed, and FLI images were acquired at different times following illumination (Fig. 7). The lifetimes are in general homogenous over the single chloroplasts and identical between most chloroplasts. The fluorescence intensity, τ_{phase} and τ_{mod} do not change significantly in 23 min for most cells. However, significant changes are observed for some cells, demonstrating changes in the fluorescence lifetimes of Chl *a* with time, and that the lifetimes as well as the changes in lifetimes are no t always identical for all cells. We did not investigate the frequency of this occurrence, because it happened only rarely (less than 1%).

3.10.2.2. Fluorescence lifetime imaging measurements are critical for interpreting fluorescence intensity measurements. There are large variations in fluorescence intensities between cells, but the distributions of τ_{phase} and τ_{mod} are quite homogeneous throughout the cells in contrast to the intensities (Fig. 8A and 8B). The large intensity variations are probably due to variations in concentration of Chl in different cells. This is an important observation. In general, unlike intensity measurements, lifetime measurements are not dependent on the excitation intensity, or the concentration of a fluorophore, in solution experiments. So any changes in lifetimes are due to environmental changes in the cells. Without the lifetime-resolved measurements, it would be impossible to interpret the intensity differences between the living cells as being mainly due to different Chl concentrations in individual cells. In our experiments with photosynthetic systems, values of fluorescence lifetimes are not in general dependent on small changes of excitation intensities, if these intensities do not vary too greatly. For instance, changing the excitation by 50% did not change τ_{phase} and τ_{mod}. Therefore, the lifetime values do not depend on the illumination profiles (Fig. 8).

However, for photosynthetic samples, differences in the excitation intensity are convoluted with the rates of photosynthetic reactions and other physiological processes. Because these physiological changes depend on the level of the irradiation, it is essential that the illumination intensity be carefully monitored so that different samples can be compared. Longer lifetimes have been observed for 'Hi' excitation intensities (Briantais *et al.*, 1972); this is due to a greater fraction of closed reaction centres, which reduces the rate constant of photochemistry.

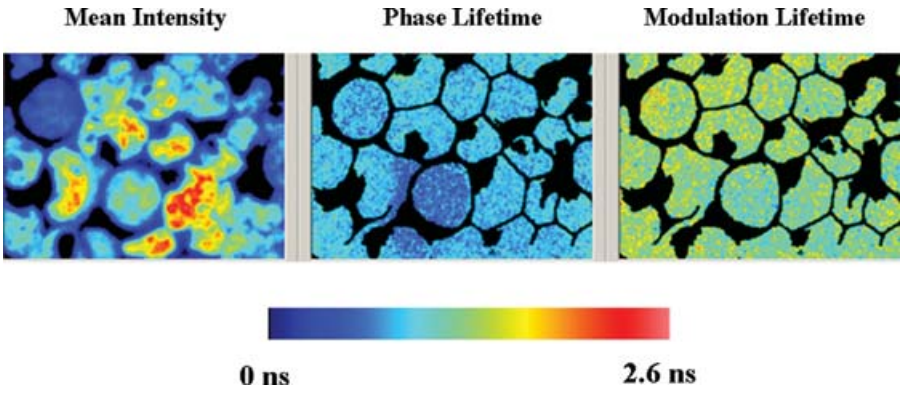

Fig. 7. Homogeneity of τ_{phase} and τ_{mod} images with large variance of the Chl *a* fluorescence intensities. Images of Chl *a* fluorescence parameters from multiple single cells of WT immobilized on an agar film. Panels are from left to right: intensity, and apparent single lifetimes calculated from the phase (τ_{phase}) and the modulation (τ_{mod}). The heterogeneity of the fluorescence intensity is not seen in the lifetime images. This shows that the intensity variance in the cells is due to differences in the concentration of Chl. For a size calibration, the average linear dimensions of WT *Chlamydomonas* cells are between 6.5 and 8 μm (Craigie & Caavalier-Smith, 1982; Bradley & Quarmby, 2005).

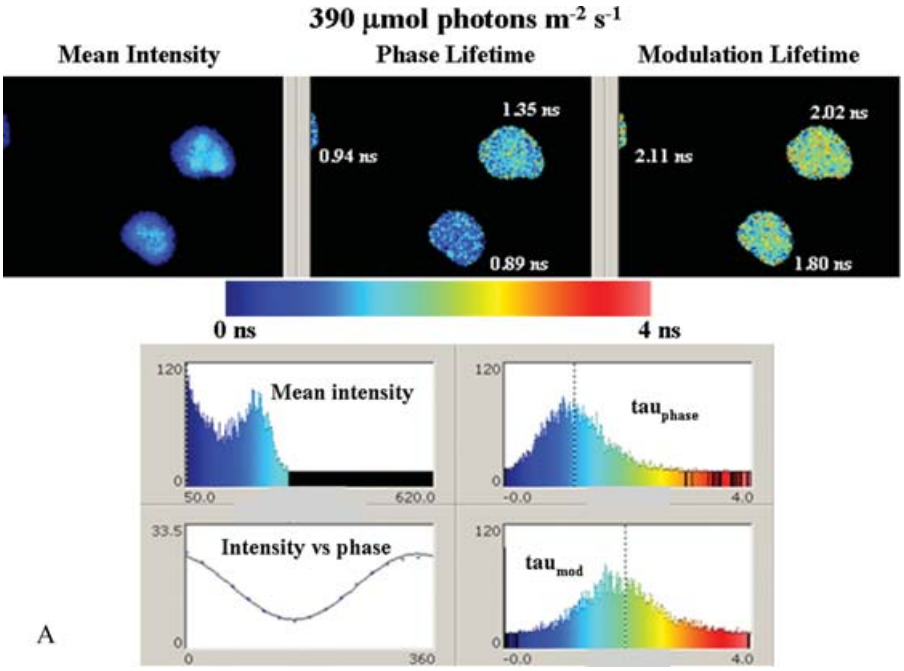

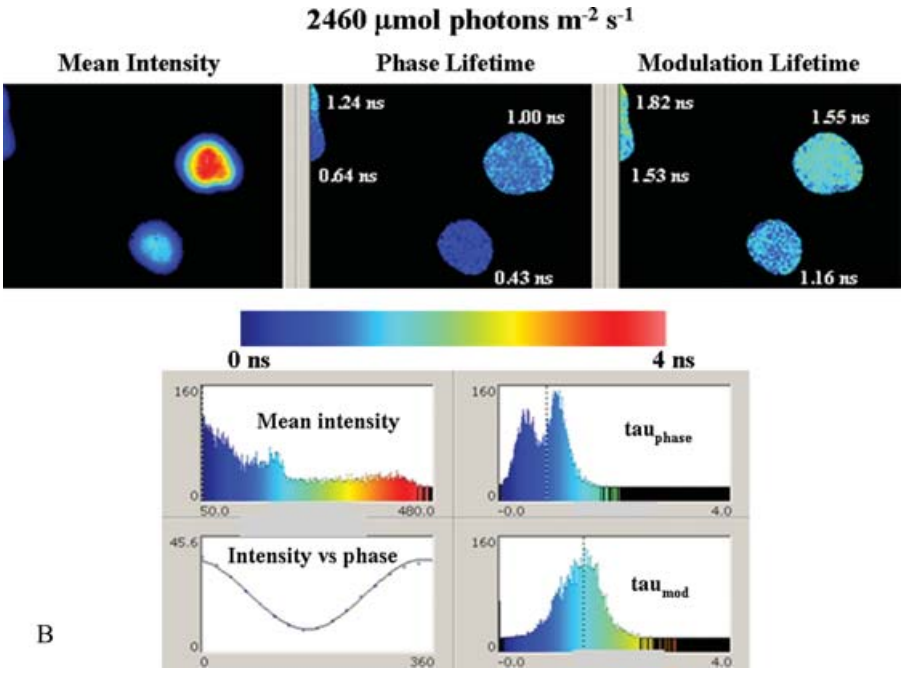

Fig. 8. Inter-cellular heterogeneities measured at two different intensities of excitation. Lifetime of Chl *a* fluorescence in single cells of *Chlamydomonas reinhardtii* measured at two different intensities of excitation: A: 390 µmol (photons) m^{-2} s^{-1} and B: 2460 µmol (photons) m^{-2} s^{-1}. Shorter lifetimes are found at the 'Hi' excitation intensity. WT cells on agar film; total irradiation time 1.96 s (at the P-level). In both A and B, the top three images are from left to right: the fluorescence intensity, τ_{phase} and τ_{mod}. The bottom four panels are (clockwise, starting from upper left): histograms of the intensity image, and the τ_{phase} and τ_{mod} images, and an example of the homodyne sine wave data averaged over selected pixels together with the fit. For a size calibration, the average linear dimensions of WT *Chlamydomonas* cells are between 6.5 and 8 µm (Craigie & Caavalier-Smith, 1982; Bradley & Quarmby, 2005).

At very high light intensities approaching sunlight (>2000 μmol photons m^{-2} s^{-1}) photoinhibition (Adir *et al.*, 2003; Osmond & Forster, 2006) sets in, and thus, the quantum yield of fluorescence is expected to decrease. Indeed, we observe a shortening of the lifetimes with increasing irradiation intensities as mentioned for the fluorescence lifetime transients above. This trend (shortening of lifetimes upon increasing the excitation intensity to that of normal sunlight) is also seen in measurements with single cells (Fig. 8) comparing different excitation intensities. The shortened lifetime values are, in all likelihood, due to photoinhibition at such high intensities.

4. Concluding remarks

In this paper, we have introduced real time, rapid FLI measurements to investigate the fluorescence response during the P-to-S-to-M transient in a photosynthetic system. Lifetime-resolved differences in the Chl *a* fluorescence between WT and xanthophyll-cycle mutants npq1 and npq2 of *Chlamydomonas reinhardtii* were investigated. The fluorescence lifetime transients show that changes in the P-to-S-to-M fluorescence transient of *Chlamydomonas reinhardtii* correlate with changes in the population distribution of fluorophores between at least two different lifetime pools. Also the lower fluorescence intensities of the npq2 mutant, which has a larger permanent concentration of zeaxanthin than either WT or npq1, are associated with shorter lifetimes, indicating dynamic quenching of excited Chl by zeaxanthin, probably by FRET.

Lifetime-resolved images of cells were carried out at peak fluorescence (P level) and during the P-to-S-to-M transient. All samples of WT, npq1 and npq2 cells showed a decline during the transient to the S level. For WT and npq1 cells, without treatment by inhibitors, this decline was followed by a rise to 'M' level at 'Hi' light intensities. This rise in the measured fluorescence intensity was not observed in any of the cells treated with DCMU, nigericin or methyl viologen. Rapid FLI measurements were necessary to determine the fluorescence lifetimes during this so-called Chl *a* fluorescence transient.

FLI data were acquired with and without the addition of DCMU (an inhibitor of electron flow), methyl viologen (an efficient electron acceptor) and nigericin (a dissipater of proton gradient); further, we made comparisons of the WT and the npq1 and npq2 mutants. We have discussed these results in light of the known physiological effects of these inhibitors. We were able to simulate the major attributes of the measured intensities for most samples from the lifetime-resolved parameters, using a two-lifetime component model. For npq2 samples without treatment with inhibitors, discrepancies between the measured fluorescence intensities and fluorescence intensities simulated from the lifetime analysis indicate additional kinetic processes during the slow transient. These dark processes were not detected in the fluorescence lifetime data. Due to the possible existence of cyclic electron flow around PS I and interaction with respiration, both NPQ and state transitions may continue to exist even with these chemicals present.

The two-component analysis of possible lifetime compositions during the transient shows that the reduction of the fluorescence intensity can be interpreted as an increase in the fraction of a short lifetime component, at the expense of the faster decaying fraction of a slower lifetime τ_2 pool of Chls. During the P-to-S transient, values of τ_2 increased concomitantly with decreasing values of the corresponding fractional species concentration a_2 and decreasing fluorescence intensity. This is interpreted in terms of a broad distribution of lifetimes centred around τ_2. The fraction of fluorophores in the τ_2 lifetime pool with shorter lifetimes exchange more readily with the τ_1 pool than the slower τ_2 components. This indicates that those molecules in the τ_2 pool which are already partially quenched are more readily transferred to the τ_1 pool during the P-to-S-to-M transient.

Fluorescence measurements of individual cells in images with multiple cells, which have been prepared identically, show significant intracellular heterogeneous fluorescence intensities. However, FLI analysis shows that the major intensity differences between cells are due to different concentrations of Chl molecules in the different chloroplasts; the lifetimes are usually (not always) the same in different cells of identical preparations. However, the lifetimes depend significantly on the physiological states of the cells (e.g. resting or swimming).

A major conclusion of our work is the notion that the distribution of Chl *a* emitters in the peripheral antennae of *Chlamydomonas reinhardtii* cluster within at least two populations, which are defined by two lifetime pools; one lifetime pool with a slower τ_2 and one with a faster τ_1.

Acknowledgments

We thank K. K. Niyogi for his generous gift of the xanthophyll-cycle mutants and G. Marriott for his loan of a Zeiss Axiovert 135 microscope. OH thanks G. Renger, H. Joachim Eichler and K. Rück-Braun at the Technische Universität, Berlin for their interest in this work. We are indebted to Dr. Glen Redford for assistance with the initial software set-up for the polar plot analysis. We also thank Dr. George Papageorgiou for his valuable suggestions during the review process. The work was financially supported by the Integrated Photosynthesis Training Grant (NSF, DBI 96-0240), start-up funds (RMC) from the UIUC Physics Department and the NIH grant (PHS 5 P41 RRO3155).

References

Adir, N., Zer, H., Shochat, S., & Ohad, I. (2003) Photoinhibition-a historical perspective. *Photosynth. Res.* **76**, 343–370.

Allen, J.F. & Forsberg, J. (2001) Molecular recognition in thylakoid structure and function. *Trends in Plant Sci.* **6**, 317–326.

Allen, J.F. (2002) Plastoquinone redox control of chloroplast protein phosphorylation and distribution of excitation energy between photosystems: discovery, background, implications. *Photosynth. Res.* **73**, 139–148.

Andersson, J., Walters, R.G., Horton, P., & Jansson, S. (2001) Antisense inhibition of the photosynthetic antenna proteins CP29 and CP26: Implications for the mechanism of protective energy dissipation. *Plant Cell* **13**, 1193–1204.

Avital, S., Brumfeld, V., & Malkin, S. (2006) A micellar model system for the role of zeaxanthin in the non-photochemical quenching process of photosynthesis—chlorophyll fluorescence quenching by the xanthophylls. *Biochimica et Biophysica Acta* **1757**, 798–810.

Bailey, E.A.J. & Rollefson, G.K. (1953) The determination of the fluorescent lifetimes of dissolved substances by a phase shift method. *J. Chem. Physics* **21**, 1315–1322.

Bassi, R., Pineau, B., Dainese, P., & Marquardt, J. (1993) Carotenoid-binding proteins of photosystem II. *Eur. J. Biochem.* **212**, 297–303.

Bean, B. (1977) Geotactic behavior of Chlamydomonas. *J. Protozool.* **24**, 394–401.

Bean, B. (1984) Microbial geotaxis In: *Membranes and sensory transduction* (ed. by G. Colombetti and F. Lenci), pp. 163–198. Plenum Press, New York.

Bennoun, P. (1982) Evidence for a Respiratory Chain in the Chloroplast. *Proc. Nat. Acad. Sci. USA* **79**, 4352–4356.

Bilger, W. & Björkman, O. (1994) Relationships among violaxanthin deepoxidation, thylakoid membrane conformation, and non-photochemical chlorophyll fluorescence quenching in leaves of cotton (Gossypium hirsutum L.). *Planta* **193**, 238–246.

Bradley, B.A. & Quarmby, L.M. (2005) A NIMA-related kinase, Cnk2p, regulates both flagellar length and cell size in *Chlamydomodas*. *J. Cell Sci.* **118**, 3317–3326.

Briantais, J.-M., Merkelo, H., & Govindjee (1972) Lifetime of the excited state *in vivo*. III. Chlorophyll during fluorescence induction in Chlorella pyrenoidosa. *Photosynthetica* **6**, 133–141.

Briantais, J.-M., Vernotte, C., Picaud, M., & Krause, G.H. (1979) A quantitative study of the slow decline of chlorophyll a fluorescence in isolated chloroplasts. *Biochimica et Biophysica Acta* **548**, 128–138.

Briantais, J.-M., Vernotte, C., Picaud, M., & Krause, G.H. (1980) Chlorophyll fluorescence as a probe for the determination of the photo-induced proton gradient in isolated chloroplasts. *Biochimica et Biophysica Acta* **591**, 198–202.

Bruce, D. & Vasilev, S. (2004) Excess light stress: multiple dissipative processes of excess excitation. In: *Chlorophyll a Fluorescence: A Signature of Photosynthesis* (ed. by G.C. Papageorgiou and Govindjee), Advances in Photosynthesis and Respiration **19**, pp. 497–523. Springer, Dordrecht.

Clayton, A.H.A., Hanley, Q.S., & Verveer, P.J. (2004) Graphical representation and multicomponent analysis of single-frequency fluorescence lifetime imaging microscopy data. *J. Microsc.* **213**, 1–5.

Clegg, R.M. & Schneider, P.C. (1996) Fluorescence lifetime-resolved imaging microscopy: a general description of the lifetime-resolved imaging measurements. In: *Fluorescence Microscopy and Fluorescent Probes* (ed. by J. Slavik), pp. 15–33. Plenum Press, New York.

Clegg, R.M., Schneider, P.C., & Jovin, T.M. (1996) Fluorescence lifetime-resolved imaging microscopy. In: *Biomedical Optical Instrumentation and Laser-Assisted Biotechnology* (ed. by A.M. Verga Scheggi, S. Martellucci, A.N. Chester and R. Pratesi), Series E: Applied Sciences **325**, pp. 143–156. Kluwer Academic Publishers, Dordrecht, Boston, London.

Clegg, R.M., Holub, O., & Gohlke, C. (2003) Fluorescence lifetime-resolved imaging: measuring lifetimes in an image. *Methods Enzymol.* **360**, 509–42.

Craigie, R.A. & Caavalier-Smith, T. (1982) Cell volume and the control of the Chlamydomonas cell cycle. *J. Cell Sci.* **54**, 173–191.

Crimi, M., Dorra, D., Bösinger, C.S., Giuffra, E., Holzwarth, A.R., & Bassi, R. (2001) Time-resolved fluorescence analysis of the recombinant photosystem II antenna complex CP29 – Effects of zeaxanthin, pH and phosphorylation. *Euro. J. Biochem.* **268**, 260–267.

Cruz, J.A., Avenson, T.J., Kanazawa, A., Takizawa, K., Edwards, G.E., & Kramer, D.M. (2005) Plasticity in light reactions of photosynthesis for energy production and photoprotection. *J. Exp. Botany* **56**, 395–406.

Delosme, R., Olive, J., & Wollman, F.A. (1996) Changes in light energy distribution upon state transitions – an in vivo photoacoustic study of the wild type and photosynthesis mutants from Chlamydomonas reinhardtii. *Biochimica et Biophysica Acta – Bioenergetics* **1273**, 150–158.

Demmig, B., Winter, K., Krüger, A., & Czygan, F.-C. (1988) Zeaxanthin and the heat dissipation of excess light energy in Nerium oleander exposed to a combination of high light and water stress. *Plant Physiol.* **87**, 17–24.

Demmig-Adams, B. (1990) Carotenoids and photoprotection in plants: a role for the xanthophyll zeaxanthin. *Biochimica et Biophysica Acta* **1020**, 1–24.

Demmig-Adams, B., Gilmore, A.M., & Adams III, W.W. (1996) Carotenoids 3: in vivo function of carotenoids in higher plants. *FASEB J.* **10**, 403–412.

Demmig-Adams, B. & Adams III, W.W. (2000) Photosynthesis–Harvesting sunlight safely. *Nature* **403**, 371–374.

Demmig-Adams, B. (2003) Linking the xanthophylls cycle with thermal energy dissipation. *Photosynth. Res.* **76**, 73–80.

Demmig-Adams, B., Adams III, W.W., & Mattoo, A.K. (Ed) (2006) *Photoprotection, Photoinhibition, Gene Regulation and Environment. Advances in Photosynthesis and Respiration.* **21** Springer, Dordrecht

Donnan, L. & John, P.C. (1983) Cell cycle control by timer and sizer in Chlamydomonas. *Nature* **304**, 630–633.

Drexhage, K.H. (1973) Structure and properties of laser dyes. In: *Dye lasers* (ed. by F.P. Schäfer), Topics in Applied Physics Series **1**, pp. 144–193. Springer, Berlin.

Elrad, D., Niyogi, K.K., & Grossman, A.R. (2002) A major light-harvesting polypeptide of photosystem II functions in thermal dissipation. *Plant Cell* **14**, 1801–1816.

Finazzi, G., Chasen, C., Wollman, F.-A., & de Vitry, C. (2003) Thylakoid targeting of Tat passenger proteins shows no DpH dependence in vivo. *EMBO J.* **22**, 807–815.

Fornshell, J.A. (1978) An experimental investigation of bio convection in 3 species of microorganisms. *J. Protozool.* 125–133.

Forti, G., Agostiano, A., Barbato, R., Bassi, R., Brugnoli, E., Finazzi, G., Garlaschi, F.M., Jennings, R.C., Melandri, B.A., Trotta, M., Venturoli, G., Zanetti, G., Zannoni, D., & Zucchelli, G. (2006) Photosynthesis research in Italy: a review. *Photosynth. Res.* **88**, 211–240.

Frank, H.A., Bautista, J.A., Josue, J.S., & Young, A.J. (2000) Mechanism of nonphotochemical quenching in green plants: energies of the lowest excited singlet states of violaxanthin and zeaxanthin. *Biochemistry* **39**, 2831–2837.

Frank, H.A., Das, S.K., Bautista, J.A., Bruce, D., Vasil'ev, S., Crimi, M., Croce, R., & Bassi, R. (2001) Photochemical behavior of xanthophylls in the recombinant photosystem II antenna complex, CP26. *Biochemistry* **40**, 1220–1225.

Gadella Jr., T.W.J., Jovin, T.M., & Clegg, R.M. (1993) Fluorescence lifetime imaging microscopy (FLIM): spatial resolution of microstructures on the nanosecond time scale. *Biophys. Chem.* **48**, 221–239.

Gilmore, A.M. & Yamamoto, H.Y. (1993) Linear models relating xanthophylls and lumen acidity to non-photochemical fluorescence quenching: evidence that antheraxanthin explains zeaxanthin-independent quenching. *Photosynth. Res.* **35**, 67–78.

Gilmore, A.M., Hazlett, T.L., & Govindjee (1995) Xanthophyll cycle-dependent quenching of photosystem ii chlorophyll a fluorescence – formation of a quenching complex with a short fluorescence lifetime. *Proc. Nat. Acad. Sci. USA* **92**, 2273–2277.

Gilmore, A.M., Shinkarev, V.P., Hazlett, T.L., & Govindjee (1998) Quantitative analysis of the effects of intrathylakoid pH and Xanathophyll cycle pigments on Chlorophyll a fluorescence lifetime distributions and intensity in thylakoids. *Biochemistry* **37**, 13582–13593.

Gilmore, A.M. & Govindjee (1999) How higher plants respond to excess light: energy dissipation in photosystem II. In: *Concepts in Photobiology : Photosynthesis and Photomorphogenesis* (ed. by G.S. Singhal, G. Renger, K.D. Irrgang, Govindjee and S. Sopory), pp 513–548. Narosa Publishers, New Delhi /Kluwer Academic Publishers, Dordrecht.

Gilmore, A.M., Itoh, S., & Govindjee (2000) Global spectral kinetic analysis of room temperature chlorophyll a fluorescence from light harvesting antenna mutants of barley. *Phil. Trans. Royal Soc. London* **B355**, 1371–1384.

Gilmore, A.M. & Yamamoto, H.Y. (2001) Time-resolution of the antheraxanthin- and pH-dependent chlorophyll a fluorescence components associated with photosystem ii; energy dissipation in Mantoniella squamata. *Photochem. Photobiol.* **74**, 291–302.

Gilmore, A.M. (2004) Excess light stress: probing excitation dissipation mechanisms through global analysis of time- and wavelength-resolved chlorophyll a fluorescence. In: *Chlorophyll a Fluorescence: A Signature of Photosynthesis* (ed. by G.C.P. a. Govindjee), Advances in Photosynthesis and Respiration **19**, pp. 555–581. Springer, Dordrecht.

Golbeck, J. (Ed) (2006) *Photosystem I: The Light-driven plastocyanin: ferredoxin oxidoreductase*. Advances in Photosynthesis and Respiration **24** Govindjee Springer, Dordrecht, 1000.

Goss, R. & Boehme, K.W. (1998) The xanthophyll cycle of Mantoniella squamata converts violaxanthin into antheraxanthin but not to zeaxanthin: consequences for the mechanism of enhanced non-photochemical energy dissipation. *Planta* **205**, 613–621.

Govindjee & Papageorgiou, G.C. (1971) Chlorophyll fluorescence and photosynthesis: Fluorescence transients. *Photophysiology* **6**, 1–46.

Govindjee, Amesz, J., & Fork, D.C. (Ed) (1986) *Light Emission by Plants and Bacteria*. Academic Press, Orlando.

Govindjee, Van de Ven, M., Preston, C., Seibert, M., & Gratton, E. (1990) Chlorophyll a fluorescence lifetime distributions in open and closed Photosystem II reaction center preparations: analysis by multifrequency phase fluorometry. *Biochimica et Biophysica Acta* **1015**, 173–179.

Govindjee, Van de Ven, M., Cao, J., Royer, C., & Gratton, E. (1993) Multifrequency cross-correlation phase fluorometry of open and closed reaction centers in thylakoid membranes and PSII-enriched membranes. *Photochem. Photobiol.* **58**, 437–444.

Govindjee (1995) Sixty-three years since Kautsky – Chlorophyll a fluorescence. *Aus. J. Plant Physiol.* **22**, 131–160.

Govindjee (2002) A role for a light-harvesting antenna complex of photosystem II in photoprotection. *Plant Cell* **14**, 1663–1668.

Govindjee & Seufferheld, M.J. (2002) Non-photochemical quenching of chlorophyll a fluorescence: Early history and characterization of two xanthophyll cycle mutants of Chlamydomonas reinhardtii. *J. Funct. Plant Biol.* **29**, 1141–1155.

Govindjee & Spilotro, P. (2002) An Arabidopsis thaliana mutant, altered in the -subunit of ATP synthase, has a different pattern of intensity-dependent changes in non-photochemical quenching and kinetics of the P-to-S fluorescence decay. *Funct. Plant Biol.* **29**, 425–434.

Govindjee (2004) Chlorophyll a fluorescence a bit of basics and history. In: *Chlorophyll a Fluorescence: A Signature of Photosynthesis* (ed. by G.C. Papageorgiou and Govindjee), Advances in Photosynthesis and Respiration **19**, pp. 1–42. Springer, Dordrecht.

Gratton, E. & Limkeman, M. (1983) A continuously variable frequency cross-correlation phase fluorometer with picosecond resolution. *Biophys. J.* **44**, 315–24.

Green, B.R. & Parson, W.W. (Ed) (2003) *Light-Harvesting Antennas in Photosynthesis* Advances in Photosynthesis and Respiration **13**. p. 544, Springer, Dordrecht.

Grondelle, R.V. & Gobets, B. (2004) Transfer and trapping of excitations in plant photosystems. In: *Chlorophyll a Fluorescence: A Signature of Photosynthesis* (ed. by G.C. Papageorgiou and Govindjee), Advances in Photosynthesis and Respiration **19**, pp. 107–132. Springer, Dordrecht.

Hamming, R.W.H. (1973) *Numerical Methods for Scientists and Engineers*. Dover Publications, Inc., New York.

Harris, E.H. (1989) *The Chlamydomonas Sourcebook: A comprehensive guide to biology and laboratory use*. Academic Press, San Diego.

Hiyama, T. & Ke, B. (1971) A new photosynthetic pigment, "P430": its possible role as the primary electron acceptor of photosystem I. *Proc. Nat. Acad. Sci. USA* **68**, 1010–1013.

Holt, N.E., Zigmantas, D., Valkunas, L., Li, X.-P., Niyogi, K.K., & Fleming, G.R. (2005) Carotenoid cation formation and the regulation of photosynthetic light harvesting, *Science* **307**, 433–436.

Holub, O., Seufferheld, M.J., Gohlke, C., Govindjee & Clegg, R.M. (2000) Fluorescence lifetime imaging (FLI) in real-time – a new technique in photosynthesis research. *Photosynthetica* **38**, 581–599.

Holzwarth, A.R. (1991) Excited-state kinetics in chlorophyll systems and its relationship to the functional organization of the photosystems. In: *Chlorophylls* (ed. by H. Scheer), pp. 1125–1151. CRC Press, Boca Raton.

Holzwarth, A.R., Mueller, M.G., Niklas, J., & Lubitz, W. (2005) Charge recombination fluorescence in photosystem I reaction centers from *Chlamydomonas reinhardtii*. *J. Phys. Chem. B.* **109**, 5903–5911.

Horton, P., Ruban, A.V., & Walters, R.G. (1994) Regulation of light harvesting in green plants: indication by non-photochemical quenching of chlorophyll fluorescence. *Plant Physiol.* **106**, 415–420.

Horton, P., Ruban, A.V., & Young, A.J. (1999) Regulation of the structure and function of the light-harvesting complexes of photosystem II by the xanthophyll cycle. In: *The Photochemistry of Carotenoids* (ed. by H.A. Frank, A.J. Young, G. Britton and R.J. Cogdell), Advances in photosynthesis and Respiration **8**, pp. 271–291. Kluwer Academic Publishers, Dordrecht.

Itoh, S. & Sugiura, K. (2004) Fluorescence of photosystem I. In: *Chlorophyll a Fluorescence: A Signature of Photosynthesis* (ed. by G.C.P. Govindjee), Advances in Photosynthesis and Respiration **19**, pp. 231–250. Springer, Dordrecht.

Jameson, D.M. & Gratton, E. (1983) Analysis of heterogeneous emissions by multifrequency phase and modulation fluorometry. In: *New directions in molecular luminescence, ASTM STP 822* (ed. by D. Eastwood), pp. 67–81. American Society for Testing and Materials, Philadelphia.

Jameson, D.M., Gratton, E., & Hall, R.D. (1984) The measurement and analysis of heterogeneous emissions by multifrequency phase and modulation fluorometry. *Appl. Spectrosc. Rev.* **20**(1), 55–106.

Joliot, P. & Joliot, A. (2002) Cyclic electron transfer in plant leaf. *Proc. Nat. Acad. Sci. USA* **99**, 10209–10214.

Joliot, P., Joliot, A., & Johnson, G. (2006) Cyclic electron transport around photosystem I. In: *Photosystem I: the light-driven plastocynanin: Ferreddoxin Oxido-reductase* (ed. by J. Golbeck), pp. 639–656. Springer, Dordrecht.

Karstens, T. & Kobs, K. (1980) Rhodamine B and Rhodamine 101 as reference substances for fluorescence quantum yield measurements. *J. Phys. Chem.* **84**, 1871–1872.

Kautsky, H. & Hirsch, A. (1931) Neue Versuche zur Kohlensäureassimilation. *Naturwissenschaften* **19**, 964.

Kramer, D.M., Avenson, T.J., & Edwards, G.E. (2004) Dynamic flexibility in the light reactions of photosynthesis governed by both electron and proton transfer reactions. *Trends in Plant Sci.* **9**, 349–357.

Krause, G.H. (1973) The high-energy state of the thylakoid system as indicated by chlorophyll fluorescence and chloroplast shrinkage. *Biochimica et Biophysica Acta* **292**, 715–728.

Lakowicz, J.R., Cherek, H., Gryczynski, I., Joshi, N., & Johnson, M.L. (1987) Analysis of fluorescence decay kinetics measured in the frequency domain using distributions of decay times. *Biophys. Chem.* **28**, 35–50.

Lakowicz, J.R. (1999) *Principles of Fluorescence Spectroscopy*. Kluwer Academic, New York.

Larkum, A.W., Douglas, S.E., & Raven, J.A. (Ed) (2003) *Photosynthesis in Algae*. Advances in Photosynthesis and Respiration **14**. Springer, Dordrecht

Lavorel, J. (1959) Induction of fluorescence in quinone-poisoned Chlorella cells. *Plant Physiol.* **34**, 204–209.

Lazar, D. (1999) Chlorophyll a fluorescence induction. *Biochimica et Biophysica Acta – Bioenergetics* **1412**, 1–28.

Li, X.P., Björkman, O., Shih, C., Grossman, A.R., Rosenquist, M., Jansson, S., & Niyogi, K.K. (2000) A pigment-binding protein essential for regulation of photosynthetic light harvesting. *Nature* **403**, 391–395.

Li, X.-P., Gilmore, A.M., Caffari, S., Bassi, R., Golan, T., Kramer, D., & Niyogi, K.K. (2004) Regulation of photosynthetic light-harvesting involves intrathylakoid pH sensing by PsbS protein. *J. Biol. Chem.* **279**, 22866–22874.

Majeran, W., Olive, J., Drapier, D., Vallon, O., & Wollman, F.A. (2001) The light sensitivity of ATP synthase mutants of *Chlamydomanas reinhardtii*. *Plant. Physiol.* **126**, 421–433.

Malkin, S., Wong, D., Govindjee & Merkelo, H. (1980) Parallel measurements on fluorescence lifetime and intensity changes from leaves during the fluorescence induction. *Photobiochem. Photobiophy.* **1**, 83–89.

Matsubara, S. & Chow, W.S. (2004) Populations of photoinactivated photosystem II reaction centers characterized by chlorophyll a fluorescence lifetime *in vivo*. *Proc. Nat. Acad. Sci. USA* **101**, 18234–18239.

Merkelo, H., Hartman, S.R., Mar, T., Singhal, G.S., & Govindjee (1969) Mode-locked lasers: Measurements of very fast radiative decay in fluorescent systems. *Science* **164**, 301–302.

Mohanty, N., Gilmore, A.M., & Yamamoto, H.Y. (1995) Mechanism of non-photochemical chlorophyll fluorescence quenching. II. Resolution of rapidly reversible absorbance changes at 530 Nm and fluorescence quenching by the effects of antimycin, dibucaine and cation exchanger. *Aus. J. Plant Physiol.* **22**, 239–247.

Mohanty, P., Papageorgiou, G.C., & Govindjee (1971) Fluorescence induction in the red agla *Porphyridium cruentum*. *Photochem. Photobiol.* **14**, 667.

Mohanty, P. & Govindjee (1973) Light-induced changes in the fluorescence yield of chlorophyll a in Anacystis nidulans. I. Relationships of slow fluorescence changes with structural changes. *Biochimica et Biophysica Acta* **305**, 95–104.

Mohanty, P. & Govindjee (1974) The slow decline and the subsequent rise of chlorophyll fluorescence transients in intact algal cells. *Plant Biochem. J.* **1**, 78–106.

Moise, N. & Moya, I. (2004a) Correlation between lifetime heterogeneity and kinetics heterogeneity during chlorophyll fluorescence induction in leaves: 1. Mono-frequency phase and modulation analysis reveals a conformational change of a PSII pigment complex during the IP thermal phase. *Biochimica et Biophysica Acta* **1657**, 33–46.

Moise, N. & Moya, I. (2004b) Correlation between lifetime heterogeneity and kinetics heterogeneity during chlorophyll fluorescence induction in leaves: 2. Multi-frequency phase and modulation analysis evidences a loosely connected PSII pigment-protein complex. *Biochimica et Biophysica Acta* **1657**, 47–60.

Moya, I., Silvestri, M., Vallon, O., Cinque, G., & Bassi, R. (2001) Time-resolved fluorescence analysis of the photosystem II antenna proteins in detergent micelles and liposomes. *Biochemistry* **40**, 12552–12561.

Müller, P., Li, X.-P., & Niyogi, K.K. (2001) Non-photochemical quenching: a response to excess light energy. *Plant Physiol.* **125**, 1558–1566.

Munday, J.C., Jr. & Govindjee (1969a) Light-induced changes in the fluorescence yield of chlorophyll a in vivo. 3. The dip and the peak in the fluorescence transient of *Chlorella pyrenoidosa*. *Biophy. J.* **9**, 1–21.

Munday, J.C., Jr. & Govindjee (1969b) Light-induced changes in the fluorescence yield of chlorophyll a in vivo. IV. The effect of preillumination on the fluorescence transient of *Chlorella pyrenoidosa*. *Biophy. J.* **9**, 22–35.

Munekage, Y. & Shikanai, T. (2005) Cyclic electron transport through photosystem I. *Plant Biotechnol.* **22**, 361–369.

Nedbal, L. & Whitmarsh, J. (2004) Chlorophyll fluorescence imaging of leaves and fruits. In: *Chlorophyll a Fluorescence; A signature of photosynthesis* (ed. by G.C. Papageorgiou and Govindjee), Advances in Photosynthesis and Respiration **19**, pp. 389–407. Springer, Dordrecht.

Niyogi, K.K., Björkman, O., & Grossman, A.R. (1997) Chlamydomonas xanthophyll cycle mutants identified by video imaging of chlorophyll fluorescence quenching. *Plant Cell* **9**, 1369–1380.

Niyogi, K.K. (1999) Photoprotection revisited: genetic and molecular approaches. *Ann. Rev. Plant Physiol. Plant Mol. Biol.* **50**, 333–359.

Niyogi, K.K., Shih, C., Chow, W.S., Pogson, B.J., DellaPenna, D., & Björkman, O. (2001) Photoprotection in a zeaxanthin- and lutein-deficient double mutant of Arabidopsis. *Photosynth. Res.* **67**, 139–145.

Osmond, B.B. & Forster, B. (2006) Photoinhibition: then and now. In: *Photoprotection, Photoinhibition, Gene Regulation and Environment* (ed. by B. Demmig-Adams, W.W.A. III and A.K. Mattoo), Advances in Photosynthesis and Respiration **21**, pp. 11–22. Springer, Dordrecht.

Oxborough, K. (2004a) Imaging of chlorophyll a fuorescence: theoretical and practical aspects of an emerging technique for the monitoring of photosynthetic performance *J. Exp. Botany* **55**, 1195–1205.

Oxborough, K. (2004b) Using chlorophyll a fluorescence imaging to monitor photosynthetic performance. In: *Chlorophyll a Fluorescence; a signature of photosynthesis* (ed. by G.C. Papageorgiou and Govindjee), Advances in Photosynthesis and Respiration **19**, pp. 409–428. Springer, Dordrecht.

Papageorgiou, G.C. & Govindjee (1968a) Light-induced changes in the fluorescence yield of chlorophyll a *in vivo*. II. *Chlorella pyrenoidosa*. *Biophys. J.* **8**, 1316–1328.

Papageorgiou, G.C. & Govindjee (1968b) Light-induced changes in the fluorescence yield of chlorophyll a *in vivo*. I. *Anacystis nidulans*. *Biophys. J.* **8**, 1299–1315.

Papageorgiou, G.C. (1975) Chlorophyll fluorescence: an intrinsic probe of photosynthesis. In: *Bioenergetics of Photosynthesis* (ed. by Govindjee), pp. 319–372. Academic Press, New York.

Papageorgiou, G.C. & Govindjee (Ed) (2004) *Chlorophyll a Fluorescence: A signature of photosynthesis* Advances in Photosynthesis and Respiration **19**, p. 818. Govindjee Springer, Dordrecht.

Polívka, T., Herek, J.L., Zigmantas, D., Åkerlund, H.E., & Sundström, V. (1999) Direct observation of the (forbidden) S-1 state in carotenoids. *Proc. Nat. Acad. Sci. USA* **96**, 4914–4917.

Polívka, T., Zigmantas, D., Sundström, V., Formaggio, E., Cinque, G., & Bassi, R. (2002) Carotenoid S-1 state in a recombinant light-harvesting complex of photosystem II. *Biochemistry* **41**, 439–450.

Redford, G.I. & Clegg, R.M. (2005a) Real-time fluorescence lifetime imaging and FRET using fast gated image intensifiers. In: *Molecular Imaging: FRET Microscopy and Spectroscopy* (ed. by A. Periasamy and R.N. Day), pp. 193–226. Oxford University Press, New York.

Redford, G.I. & Clegg, R.M. (2005b) Polar plot representation for frequency-domain analysis of fluorescence lifetimes. *J. Fluores.* **15**, 805–815.

Rees, D., Noctor, G., Ruban, A.V., Crofts, J., Young, A., & Horton, P. (1992) pH-dependent chlorophyll fluorescence quenching in spinach thylakoids from light treated or dark-adapted leaves. *Photosynth. Res.* **31**, 11–19.

Rochaix, J.-D., Goldschmidt-Clermont, M., & Merchant, S. (Ed) (1998) *The Molecular Biology of Chloroplasts and Mitochondria in Chlamydomonas*. Advances in Photosynthesis and Respiration **7**. Springer, Dordrecht.

Schansker, G., Tóth, S.Z., & Strasser, R.J. (2005) Methylviologen and dibromothymoquinone treatments of pea leaves reveal the role of photosystem I in the Chlorophyll a fluorescence rise OJIP. *Biochimica et Biophysica Acta* **1706**, 250–261.

Schreiber, U. (2004) Pulse-amplitude-modulation (PAM) fluorometry and saturation pulse method: an overview. In: *Chlorophyll a Fluorescence: A Signature of Photosynthesis* (ed. by G.C. Papageorgiou and Govindjee), Advances in Photosynthesis and Respiration **19**, pp. 279–319. Springer, Dordrecht.

Sjöback, R., Nygren, J., & Kubista, M. (1995) Absorption and fluorescence properties of fluorescein. *Spectrochimica Acta Part A-Molecular Spectroscopy* **51**, L7-L21.

Steffen, R., Christen, G., & Renger, G. (2001) Time-resolved monitoring of flash-induced changes of fluorescence quantum yield and decay of delayed light emission in oxygen-evolving photosynthetic organisms. *Biochemistry* **40**, 173–180.

Stirbet, A., Govindjee, Strasser, B.J., & Strasser, R.J. (1998) Chlorophyll a fluorescence induction in higher plants – modelling and numerical simulation. *J. Theor. Biol.* **193**, 131–151.

Sueoka, N. (1960) Mitotic replication of deoxyribonucleic acid in *Chlamydomonas reinhardi*. *Proc. Nat. Acad. Sci. USA* **46**, 83–91.

Takahashi, H., Iwai, M., Takahashi, Y., & Minagawa, J. (2006) Identification of the mobile light-harvesting complex II polypeptides for state transitions in Chlamydomonas reinhardtii. *Proc. Nat. Acad. Sci. USA* **103**, 477–482.

Velthuys, B.R. (1981) Electron-dependent competition between plastoquinone and inhibitors for binding to photosystem II. *Federation Euro. Biochem. Soc. (FEBS) Lett.* **126**, 277–281.

Vogel, M., Rettig, W., Sens, R., & Drexhage, K.H. (1988) Structural relaxation of rhodamine dyes with different N-substitution patterns: a study of fluorescence decay times and quantum yields. *Chem. Phys. Lett.* **147**, 452–460.

Von Hippel, A.R. (1954) *Dielectrics and Waves*. The M.I.T. Press, Cambridge.

Weber, G. (1981) Resolution of the fluorescence lifetimes in a heterogeneous system by phase and modulation measurements. *J. Phys. Chem.* **85**, 949–953.

Wentworth, M., Ruban, A.V., & Horton, P. (2000) Chlorophyll fluorescence quenching in isolated light harvesting complexes induced by zeaxanthin. *FEBS Lett.* **471**, 71–74.

Wraight, C.A. (1981) Oxidation-reduction physical chemistry of the acceptor quinone complex in bacterial photosynthetic reaction centers: evidence for a new model of herbicide activity. *Israel J. Chem.* **21**, 348–354.

Wydrzynski, T. & Satoh, K. (Ed) (2005) *Photosystem II: The Light-Driven Water: Plastoquinone Oxidoreductase*. Advances in Photosynthesis and Respiration **22**. Springer, Dordrecht.

Yamamoto, H.Y. (2006) A random walk to and through the xanthophyll cycle. In: *Photoprotection, Photoinhibition, Gene Regulation and Environment* (ed. by B. Demmig-Adams, W.W.A. III and A.K. Mattoo), Advances in Photosynthesis and Respiration **21**, pp. 1–10. Springer, Dordrecht.